J. Fluid Mech. (2002), *vol.* 462, *pp.* 43–77.
DOI: 10.1017/S0022112002008546 Printed in the United Kingdom

Influence of vortex-pairing location on the three-dimensional evolution of plane mixing layers

By JORDI ESTEVADEORDAL[1] AND STANLEY J. KLEIS[2]

[1]Innovative Scientific Solutions Inc., Dayton, OH 45440, USA

[2]Department of Mechanical Engineering, University of Houston, Houston TX 77204, USA

(Received 15 September 2000 and in revised form 8 January 2002)

Detailed three-dimensional measurements of the first vortex pairing of a large plane mixing layer reveal excitation of several three-dimensional instability modes. Time evolution in three-dimensional space (x, y, z, t) shows how the two-dimensional rollers become three-dimensional as they approach each other and that the linear growth of at least two instability waves leads to a spanwise periodic pairing. The results are based on phase-locked measurements made in three-dimensional spatial grids, with a mesh spacing of 8.5% of the fundamental instability wavelength. Spanwise-uniform, periodic acoustic excitation stabilizes the most probable two-dimensional natural features – roll-up and first pairing. The second subharmonic is added to study the effect of alternate streamwise pairing locations on the three-dimensional characteristics of vortex pairing. Velocities are measured using hot-wire anemometry, and the coherent structures are reconstructed from the ensemble-averaged vorticity field.

Vortex pairing is shown to initiate through local 'bridging' at the maxima of periodic spanwise undulations. The undulations result from linear amplification of various instability modes on pairing rollers having different strengths. Bridging results from the change of the relative phase between the spanwise undulations of the pairing rollers from in-phase (due to the initial translative mode) to out-of-phase (due to the amplification of bulging-like and non-axisymmetric modes). It is found that when pairing occurs sufficiently far upstream, only axisymmetric waves are amplified and the evolution results in axisymmetric merging. In contrast, when pairing occurs sufficiently far downstream, both axisymmetric and non-axisymmetric waves are amplified and the evolution results in non-axisymmetric merging.

The results indicate that vortex pairing is accompanied by the counter-rotating pairs of secondary structures ('streamwise vortices' or 'ribs') located in the mixing-layer braids and residing in the valleys of the spanwise-roller waves. Time evolution of these secondary structures shows that they move in the transverse direction, following the rollers.

1. Introduction

The origin and evolution of mixing-layer coherent structures (large-scale vortical regions with spatially correlated vorticity) have been studied extensively. The primary coherent structures (Brown & Roshko 1974; Winant & Browand 1974), also termed spanwise vortices or rollers, result from the two-dimensional evolution of the mixing

layer and are initially two-dimensional in the absence of external spanwise perturbations. These structures can persist quasi-two-dimensionally to far-downstream locations after their first pairing (Wygnanski *et al.* 1979; Tung & Kleis 1996), although some studies (Chandrsuda *et al.* 1978) have found that they quickly become three-dimensional. Breidenthal (1980, 1981) found that when these structures are formed from a three-dimensional splitter plate, they quickly relax to their characteristic two-dimensional structure, although their spanwise non-uniformities are amplified as they are convected downstream. The secondary coherent structures, also termed streamwise vortices or 'ribs' (Hussain 1986), result from the three-dimensional evolution of the mixing layer (Lin & Corcos 1984; Bernal & Roshko 1986; Metcalfe *et al.* 1987); they reside in the braids arranged as counter-rotating pairs. These secondary structures can become apparent during roll-up (Huang & Ho 1990; Bell & Mehta 1992; LeBoeuf & Mehta 1996) or during pairing of the rollers (Pierrehumbert & Widnall 1982; Tung & Kleis 1996), depending on the initial conditions.

Some studies have reported that the rollers can be forced initially to be highly three-dimensional, having strong streamwise and transverse vorticity components and thereby losing their identity as spanwise rollers. This is the case for the strong short-wavelength spanwise forcing used in the experiments of Nygaard & Glezer (1994) and the simulations of Comte, Lesieur & Lamballais (1992) and Collis *et al.* (1994). Rogers & Moser (1992, 1993) and Moser & Rogers (1993) simulated up to three pairings of the temporally growing mixing layer by applying initial perturbations having different amplitudes and phases; they found that the resulting evolutions can be diverse, which explains the diversity of the experimental results. Some experimental studies on spanwise-unforced plane mixing layers (Estevadeordal & Kleis 1999*a*, *b*) have revealed 'core instabilities' during first vortex pairing and 'double-helical' second pairing. Studies using artificial spanwise forcing at the splitter plate have shown that the secondary structures can appear even before the roll-up (Lasheras, Cho & Maxworthy 1986; Lasheras & Choi 1988; Nygaard & Glezer 1991; Bell & Mehta 1993). In these studies the rollers became three-dimensional as soon as they were generated, with alternating bending slopes that are consistent with spanwise forcing. Although most of these studies with three-dimensional rollers found secondary structures in the braids, some simulations (Schoppa, Hussain & Metcalfe 1995) revealed that three-dimensional-roller evolution from the bulging mode can occur without these structures.

Early experimental studies on the spanwise structure of spatially evolving plane mixing layers (Browand 1966) reported the presence of high frequencies, which were harmonics of the initial two-dimensional Kelvin–Helmholtz wave. These frequencies were thought to be produced by secondary instabilities, the evolution of which produces strong nonlinear distortions and non-periodic spanwise structure. Browand & Troutt (1980, 1985) later related these frequencies to vortex pairing through 'branchings, ends, and terminations' within pairing rollers. The spanwise measurements of Miksad (1972) showed strong two-dimensionality up to the region where the first subharmonic of the initial wave was triggered. As the subharmonic grew, three-dimensional distortions appeared. In agreement with the simulations of Benney & Lin (1960), Miksad's (1972) interpretation was that longitudinal vortex structures along the streamwise direction and secondary instabilities follow the subharmonic growth. From that point, much attention was given to the spanwise structure of the mixing layer – especially regarding the primary and secondary coherent-structure dynamics during pairing. However, elucidation of the processes taking place within pairing rollers is still lacking. The current study presents a novel view of the first vortex

pairing, unveils new spanwise characteristics, and correlates observations reported in previous studies by Browand & Troutt (1980, 1985), Pierrehumbert & Widnall (1982), Rogers & Moser (1992), Moser & Rogers (1991, 1993), Schoppa *et al.* (1995), Bell & Mehta (1992), LeBoeuf & Mehta (1996), Tung & Kleis (1996), and Estevadeordal & Kleis (1999*a*, *b*).

For studying the onset of three-dimensionality, a fine three-dimensional spatial grid was used (resolution of 8.5% of the fundamental wavelength). The effect of the streamwise location on the two-dimensionality of the rollers during first pairing was investigated by introducing the second subharmonic in the acoustic wave; this generates two vortex pairing configurations at different streamwise locations, each having rollers of different strengths (Estevadeordal & Kleis 1999*c*). The second subharmonic was also introduced because it stabilizes the second pairing, which will be the focus of a future investigation.

Low-level forcing (maximum 82 dB SPL) provided a two-dimensional known perturbation for triggering and stabilizing (Ho & Huang 1982) the most probable events – roll-up and pairings (Hussain 1986). Forcing localizes the events at fixed streamwise distances and, therefore, eliminates the randomness and jitter associated with a natural mixing layer; it also smears (or eliminates) other types of interactions (e.g. triplets). As a consequence, the stabilized events take place and evolve at the same streamwise locations at all times, and flow features can be educed using phase-average techniques. One of the limitations of phase-averaging is that conclusions regarding events that are not phase-locked, such as those associated with small scales and turbulence, should be drawn carefully.

2. Experimental set-up

2.1. *Facility and conditions*

The study was carried out in the mixing-layer facility of the Turbulent Shear Flow Laboratory of the University of Houston; this facility was designed to provide a plane, large, low-speed mixing layer as free as possible from environmental disturbances and end effects. The two-stream, closed-loop wind tunnel is shown schematically in figure 1. The mixing layer originates after the two streams merge at the knife edge of the splitter plate – the end of the splitter wall that separates the two legs of the tunnel. Because of the large size of the mixing layer, high Reynolds numbers can be achieved with low free-stream velocities (maximum attainable value is $30\,\mathrm{m\,s^{-1}}$) and thick boundary layers that can be maintained laminar for free-stream velocities up to $15\,\mathrm{m\,s^{-1}}$ through a boundary-layer control system located at the splitter plate. The resulting flow is suitable for hot-wire measurements with good spatial resolution. A traversing system for three-dimensional probe positioning is located on the roof of the tunnel test section. Traverse movement in all three directions is free of backlash, with a resolution of 0.0254 mm. The test section extends 1.05 m in the transverse direction (y), 1.65 m in the spanwise direction (z), and 12 m in the streamwise direction (x). In the present experiments the velocities of the streams were set one at $5.5\,\mathrm{m\,s^{-1}}$ and the other at $1.8\,\mathrm{m\,s^{-1}}$, with zero streamwise pressure gradient. For the high- and low-speed sides, boundary-layer-displacement thickness was 0.298 and 0.380 cm, and momentum thickness was 0.108 and 0.165 cm, respectively. Typical r.m.s.-velocity fluctuation levels in the free-stream region of the test section were $\sim 0.07\%$ of the mean flow. Under these conditions the natural fundamental frequency of the mixing layer was 119 Hz (readily observed from the spectrum of the hot-wire signal). The

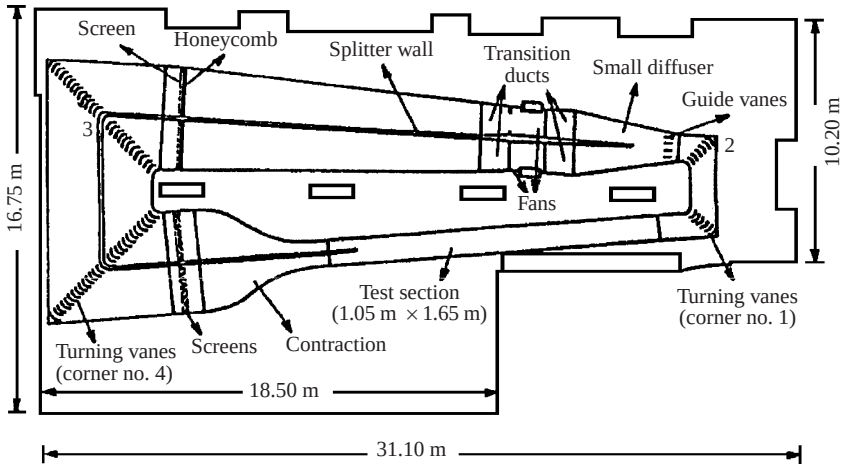

FIGURE 1. Wind-tunnel schematic.

time-averaged streamwise velocity profile of the mixing layer quickly relaxed to a hyperbolic-tangent distribution in the transverse direction. The momentum thickness of the stabilized mixing layer increased from 0.15 cm at the roll-up (plateau centred at 13 cm downstream of the knife edge) to 0.45 cm at the first pairing (plateau centred at 30 cm downstream of the knife edge). Based on the velocity difference and the local momentum thickness, the Reynolds numbers corresponding to these two events are 365 and 1095, respectively.

Velocities were measured using constant-temperature hot-wire anemometry, with a TSI T1.5 '×' probe connected to a TSI IFA-100 Intelligent Flow Analyzer for signal conditioning (offset, gain, and low-pass filtering) of the bridge output signal. The overheat ratio was 1.4. The sensors were made of tungsten wire and were 1.4 mm in length and 5 μm in diameter. The separation between the wires of the probe was 1 mm. The probe was oriented with the plane of the wires in the (x, y)-plane for measuring the streamwise (u) and transverse (v) velocities and was rotated 90° to the (x, z)-plane for measuring the streamwise (u) and spanwise (w) velocities. The hot-wire probe was calibrated against a Pitot tube in the free-stream region of the tunnel and was also yaw calibrated to determine the effective angle between the wires. The velocity measurements were corrected for velocity gradients in the direction normal to the plane of the wires. When the gradient is non-zero, the effective cooling velocity for the two wires is different, especially if the velocity gradients are large (such as within the mixing layer). The correction, based on a first-order Taylor's series expansion about a point midway between the wires, was applied for v and w. The gradients were evaluated by a finite-difference scheme (centered-second-order). The calibration was performed after the tunnel had been in operation for several hours (typically about 5) to allow conditions in the tunnel to settle. The temperature was measured and used to compensate for temperature variations during the experiment (typically $< 0.5\,^{\circ}\mathrm{C}$).

The flow was phase-locked with an acoustic wave that also provided the triggering signal (and reference) for data acquisition. The wave, $W(t)$, was the sum of three sinusoidal waves – the fundamental and its first and second subharmonics – and had the following general form:

$$W(t) = A_0 \sin(2\pi f t - \phi_0) + A_1 \sin(\pi f t - \phi_1) + A_2 \sin\left(\pi \tfrac{1}{2} f t - \phi_2\right), \qquad (2.1)$$

where A_0, A_1 and A_2 are the amplitudes and ϕ_0, ϕ_1 and ϕ_2 are the phases of

the fundamental, the first-subharmonic wave, and the second-subharmonic wave, respectively. The second subharmonic was used as the phase reference ($\phi_2 = 0$). The fundamental frequency corresponded to the initial instability frequency of the mixing layer (roll-up), and the first and second subharmonics corresponded to the frequencies of the first and second pairings, respectively. As explained earlier, in this study the second subharmonic was used to alter the location of alternate first pairings (Estevadeordal & Kleis 1999*c*).

The wave was generated by means of a single-board computer. The printed-circuit board was connected to a Macintosh computer for programming and data input. A BASIC program computed the wave form according to the parameters entered (amplitudes and phases). The program called a machine-language routine that repeatedly scanned a cycle of the stored wave form to a 12 bit D/A converter. The amplitude of the analog wave could be changed via a variable-gain output amplifier. The output signal was connected to a loudspeaker through a power stereo amplifier. One point in the cycle of the digital wave was used to provide a triggering pulse; its frequency was the smallest of the wave components ($f/4$). The design allowed the adjustment of the amplitudes, frequencies, and phases of the wave components. Variations of these parameters can lead to different flow patterns. All measurements in the present study were based on the same amplitudes and phase differences (near zero) for the three wave components to satisfy the purposes of the investigation (stabilization of the first vortex pairing as near as possible to the knife edge and at two downstream locations). As pointed out by Tung (1992), the efficiency of the acoustic excitation in a close-loop wind tunnel is high, regardless of the location of the source inside the tunnel. In the present study, the speaker was located 6 m downstream from the tip of the knife edge – far from the area where the data were taken (within 0.6 m of the tip of the knife edge) to ensure that the speaker box would not interfere with the flow of interest. This location also provided a spanwise-uniform (two-dimensional) acoustic perturbation at the knife edge (the point where the acoustic wave produces a hydrodynamic effect); this was verified by checking the wave along the knife edge using a microphone (the wave amplitude and phase were spanwise uniform within 0.5%). In addition, the sound level was measured at different locations in the test section, and it remained spanwise uniform (82 dB SPL at the knife edge). Thus, the acoustic wave introduced a small spanwise-uniform perturbation in the flow at the knife edge.

The data were acquired by a MASSCOMP MC5400 computer featuring five clocks for synchronization of the data acquisition, a traversing system, and external triggering devices. The A/D converter had 16 channels and 12 bits for a voltage range of -10 to $+10$ V.

2.2. *Measurement techniques*

The acoustic wave stabilized the flow and set a phase reference for the data acquisition and ensemble-average (or phase-average) over a number of realizations. Although the excitation provides stabilization of the flow (events are fixed in time and space), a larger number of ensembles is needed downstream because of the increase in flow jitter. The main sources of jitter are the differences in the arrival time of the structures at the measurement point and the natural differences between realizations due to transition to turbulence. A flow quantity (u) can be decomposed into a phase-coherent part ($\langle u \rangle$) and a phase-random part (u_r). Different decompositions of the ensemble-average of a quantity can be found in Hussain (1986).

The reconstruction of the vorticity field, which was used for the recognition (and definition) of coherent structures in the flow, was computed from the ensemble-

averaged velocity field using a centred finite-difference scheme (second order). The representation of vortical structures through iso-surfaces has been proven to be proper for mixing-layer studies (Jeong & Hussain 1995). Since detailed and accurate measurements were sought, the time-evolving velocity field was measured on three-dimensional spatial grids. A set of samples from all points on the measurement grid at any given time delay from the trigger represents a snapshot of the velocity and vorticity fields at that particular phase. The temporal evolution of the spatial fields is reconstructed from a sequence of phases from all time traces of the grid. This technique has been used in the past for two-dimensional (Zaman & Hussain 1981; Estevadeordal & Kleis 1999*c*) and three-dimensional (LeBoeuf & Mehta 1996) mixing-layer studies. In the present experiments, data were acquired at 20 phases of the longest period – the second subharmonic – for capturing the two pairing configurations under study. These two configurations occur during the first and second half of the second-subharmonic period, respectively. The first grid captures the passage of two rollers during prepairing (phases indicated as 0–5) and the pairing that occurs closer to the knife edge (phases 12–17). The second grid captures the passage of the roller merged closer to the knife edge (merged 1) (phases 1–5) and the passage of the roller merged farther downstream (merged 2) (phases 12–14). The relation between the phases of the second-subharmonic cycle and the pairing locations is discussed in greater detail by Estevadeordal & Kleis (1999*c*). The present study focused on the three-dimensional characteristics of the two first vortex-pairing configurations and the merging configurations that resulted, with emphasis on the phases indicated above. These phases clearly captured (i) the pairing that occurred closer to the knife edge and its spanwise variations that occurred during the pairing process and (ii) the two merging structures that resulted.

The ensemble-averaged vorticity field is displayed through iso-contours and their interpolated images for two-dimensional presentation and through iso-surfaces for three-dimensional presentation. In all figures the tick marks on the axes correspond to the actual measurement grid used in data acquisition. The units are dimensional to emphasize the physical dimensions of the coherent structures. Non-dimensionalization can be easily computed by dividing the transverse distances by the high-speed-side boundary-layer momentum thickness ($\theta_H = 0.1\,\mathrm{cm}$), the streamwise and spanwise distances by the fundamental wavelength ($\lambda_0 = 3\,\mathrm{cm}$), and the vorticity by the maximum time-averaged vorticity ($\partial U/\partial y = 1150\,\mathrm{s}^{-1}$); the length scales are related through the Strouhal number ($\theta_H/\lambda_0 = 0.03$). Negative y corresponds to the high-speed side. The measurement-grid spatial resolution is 0.254 cm in each direction. The streamwise distance is referenced to the tip of the knife edge of the splitter plate ($x = 0$). The number of ensembles is 100 for all cases. The measurement locations are summarized in table 1.

The spatial uncertainty was taken to be the traverse-motion resolution. The uncertainty in velocity was calculated from the uncertainty of the voltages from the hot wire (given by the A/D conversion and multiplied by 2 to account conservatively for the noise) through the calibration curve. The increments in velocity were conservatively estimated by the maximum vorticity multiplied by the spatial step. The maximum was that for the spanwise vorticity, $42\,\mathrm{s}^{-1}$. The calculation did not take into account other factors (assumed to have negligible uncertainty) such as the separation of the wires in the probe and their angle (bias error was removed), which would increase the value, and the gain of the AC coupling, which would decrease it. The highest uncertainty in the estimation of the ensemble-averaged spanwise vorticity was 4% for typical values of the variables measured.

First pairing	Grid points ($x \times y \times z \times t$)	Streamwise range x (cm)	Transverse range y (cm)	Spanwise range z (cm)	Sampling rate (Hz)	Number of ensembles
Two-dimensional grid	$51 \times 21 \times 1 \times 20$	20.57 to 32.77	−1.00 to 3.56	$z = 0$	400	100
Three-dimensional grids	$23 \times 23 \times 23 \times 20$	21.34 to 26.92	−2.29 to 3.30	−3.05 to 2.54	595	100
	$23 \times 23 \times 23 \times 20$	26.42 to 32.00	−1.52 to 4.06	−3.05 to 2.54	595	100

TABLE 1. Measurement conditions

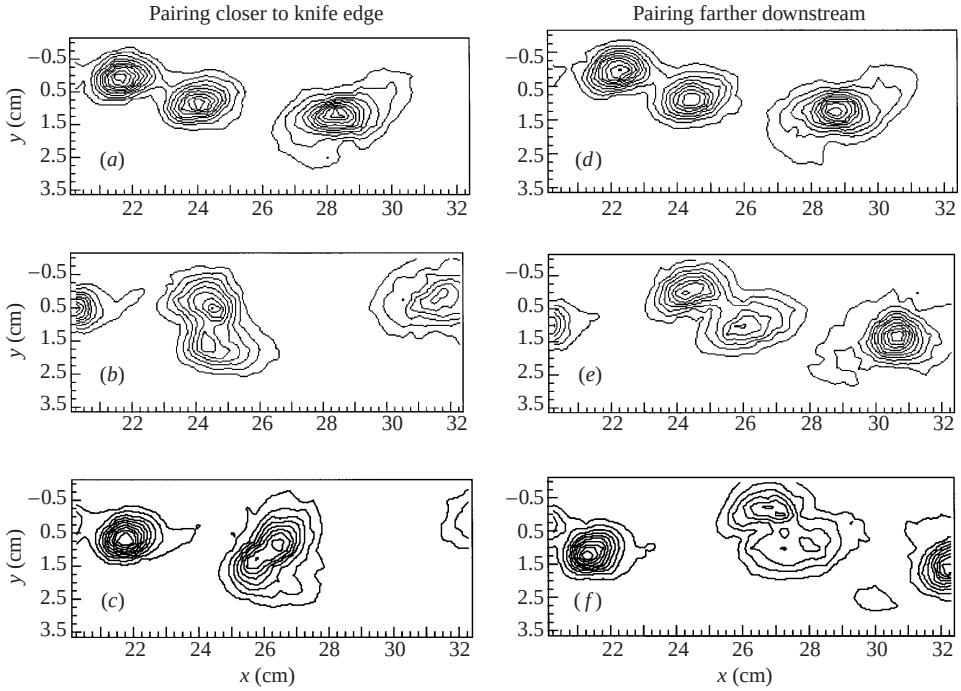

FIGURE 2. Downstream locations of two first-pairing configurations in one second-subharmonic cycle in the (x, y)-plane. Iso-contours of phase-averaged spanwise vorticity ($\langle\omega_z\rangle$, s^{-1}) in (x, y) at $z = 0$ cm; $\langle\omega_z\rangle = 75$ to $800\,s^{-1}$ @ $75\,s^{-1}$ (@ denotes the interval).

3. Vortex pairing: interaction of three-dimensional instabilities

Under the present conditions the rollers undergo two distinct first-pairing configurations. The second-subharmonic signal changes the location of the first pairing and allows the study of two pairing configurations (Estevadeordal & Kleis 1999*c*). After the roll-up every fourth vortex is more shifted toward the high-speed side than the others; thus, pairing occurs differently in alternate pairs and at different downstream distances, as shown in figure 2. This figure displays six frames of a second-subharmonic cycle. The pairing rollers revolve around each other by mutual induction with progressive merging. At the pairing locations ($\sim$ 25 cm and 28 cm in frames (*c*) and (*f*), respectively), defined as the 90° position (as in Ho & Huang 1982), merging is $\sim$ 50% complete. The merged structure continues to revolve as it travels downstream in a fashion similar to that of the original rolled-up vortices, including the two spiraling arms.

The contours also show that the low-speed-side roller is more disorganized than the high-speed-side roller, especially in the farther downstream pairing (frames (*d–f*)); it has a lower peak spanwise vorticity and a slightly larger size. From a two-dimensional perspective, an explanation is that upon pairing, this 'older' roller has been diffusing for a longer time than the high-speed roller and, thus, has a lower peak vorticity and a larger size (Estevadeordal & Kleis 1999*c*). Investigation of the influence on three-dimensionality as well as the three-dimensional implications of the low-speed roller being 'older/weaker' are objectives of this study. Phase decorrelation could also influence the ensemble-averaging results if, for example, the pairing configurations were occurring at very different downstream locations. In the present investigation

the two pairing configurations occur at very similar downstream locations and are expected to be equivalently phase-locked.

To study the repeated large-scale events, phase-averaged measurements were made on the two three-dimensional grids (table 1) that encompass the roll-up and the first pairings. The grids are streamwise-consecutive and track the rollers from the end of the roll-up to the end of the first mergings. The measurements on these grids capture distinct features of the two vortex-pairing locations which, for a given fundamental and first subharmonic, are changed by the second subharmonic. The results also show the relative position of the rollers and the secondary structures.

3.1. *Roller instabilities*

The slight variation between the spanwise sections (e.g. as shown in figure 3*a–c*) as well as the almost straight iso-vorticity lines in (y, z) sections through the middle of the rollers (as shown in figure 3*d*) reveal that the rollers are quasi-two-dimensional initially. However, two small deviations can be seen – the periphery (area with low iso-vorticity) exhibits mild waviness, and the centre of the core has a small kink (small perturbation or deviation producing a small continuous curvature on the iso-vorticity lines) near $z = 1.5$ cm. The peripheral waviness, corresponding to a very low value of spanwise vorticity, has a wavelength on the order of $0.5\lambda_0$ and is consistent with amplification of a perturbation on a sinusoidal spanwise wave (translative instability) and formation of streamwise structures in the braid. Three-dimensional measurements will most effectively determine the origin of this amplification and its evolution as the rollers approach each other. The kink is due to an upstream localized perturbation (small imperfection in the splitter plate). The results of previous studies have indicated that kinks from defects in the facility amplify the inherent instabilities of the mixing layer (Jimenez 1983; Bernal & Roshko 1986; Tung & Kleis 1996; Estevadeordal & Kleis 1999*a*, *b*) and that the mixing-layer instabilities tend to seek the preferred sites provided by the largest perturbations. This was confirmed, for instance, when various experimental set-ups produced the same instability configurations, although the sites for preferred growth were different. It is noteworthy that these local perturbations are small and lead to instabilities, with initial growth being consistent with linear-theory predictions (Metcalfe *et al.* 1987; Rogers & Moser 1992). The fact that the perturbation location is fixed facilitates the eduction of three-dimensional instabilities through phase-averaging experiments that use two-dimensional forcing only. The three-dimensional motions occur at specific locations and are also phase-locked. For example, this permits the study of the streamwise structures of the braid using two-dimensional forcing (Tung & Kleis 1996). The present results identify, by means of the spatial grid, the processes by which two-dimensional rollers become increasingly three-dimensional and the instabilities involved as they approach each other.

Figure 4 shows the spanwise vorticity profiles in the transverse direction for the roller of figure 3 at eight equally spaced z-locations. The peak values are lower near the kink location. The profiles are approximately Gaussian, and the area with vorticity (roller core) ranges from -0.5 to 2.0 cm. The area with a core vorticity that is higher than $\sim 50\%$ of the peak is called the roller centre; its diameter is ~ 1 cm at this stage, and it is denoted by a. The remainder is called the roller periphery and extends from the centre end to the region with no vorticity; at this stage it has an outside diameter of ~ 2.5 cm, is ~ 0.75 cm thick, and is denoted by b. These two areas serve as a reference for the slices from the three-dimensional plots presented in this paper. The waves on the two sides of the periphery of the roller (one centred around $y = 0$ and the other around $y = 1.5$ cm) appear to be in-phase and have a very low value

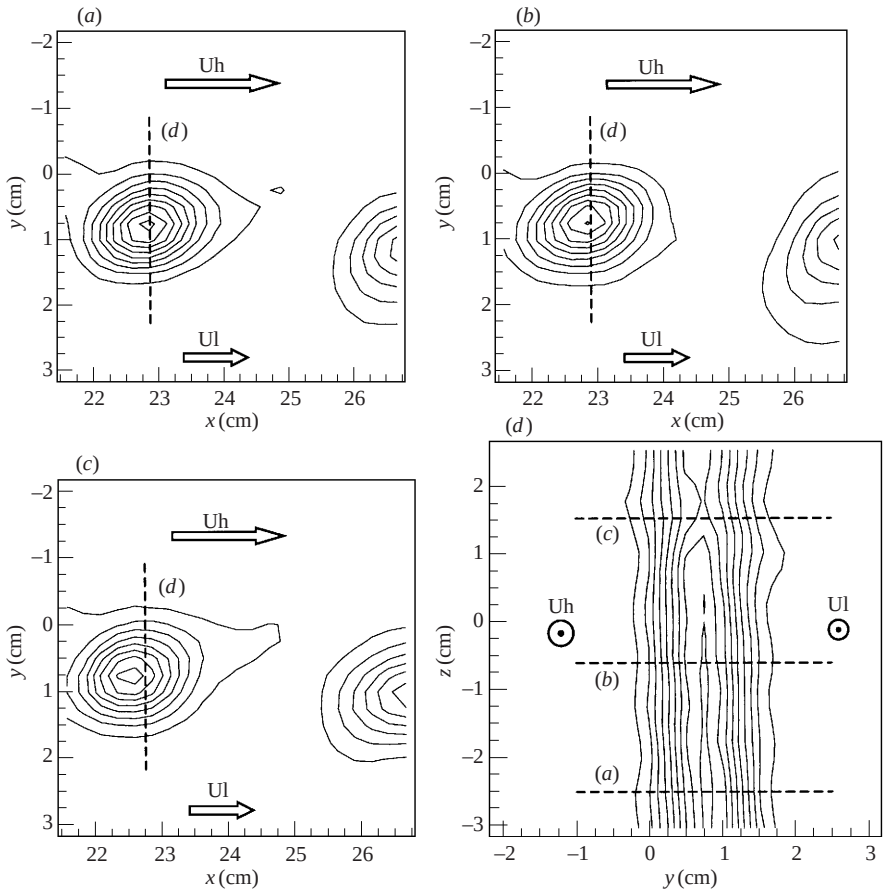

FIGURE 3. Initial quasi-two-dimensional rollers preceding pairing. Iso-contours of phase-averaged spanwise vorticity. Sections (x, y) at (a) $z = -2.5$ cm, (b) $z = -0.5$ cm, (c) $z = 1.5$ cm. Section (y, z) at (d) $x = 22.75$ cm. $\langle\omega_z\rangle = 75$ to 800 @ 75 s^{-1}. High-speed (Uh) and low-speed (Ul) sides indicated by arrows. Sections indicated by dashed lines.

of vorticity. The dashed lines that indicate z-locations aid the observation that the peaks and valleys of the two peripheries are in-phase.

The persistence and extent of quasi-two dimensionality at pairing are first presented through spanwise sections through the rollers as they continue to approach each other. These sections were chosen to show the spanwise variations for the two pairing locations (figure 5). Both locations show that at some spanwise locations, pairing is complete (Ho & Huang 1982) (b and d), and at others it is not (e.g. a and f). The farther downstream pairing (d–f) appears to be more disorganized than the upstream pairing (a–c); the vorticity values are also much lower than those associated with the pairing that occurs closer to the knife edge. Even though there are spanwise variations during pairing, spanwise sections corresponding to merging (figure 6) indicate that the resulting merging structure remains quasi-two-dimensional and axisymmetric, consistent with the results of studies on the inhibition of three-dimensionality growth during pairing (Metcalfe *et al.* 1986). However, conclusions regarding this inhibition should be drawn carefully from these phase-averaged data because small scales could exist that are not phase-locked. The merging that takes place farther downstream (d–f) appears to be less two-dimensional, axisymmetric, and organized than that

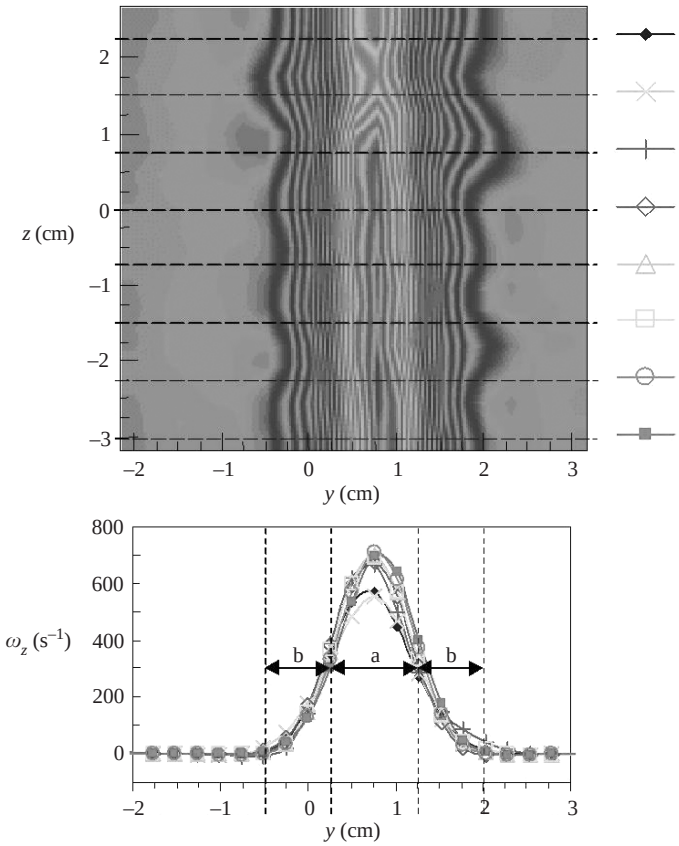

FIGURE 4. Spanwise-vorticity profiles in the transverse direction for the roller of figure 3 at eight z-locations ($z = 2.25$ to -3.00 @ 0.75 cm). Lower peak values occur near the 'kink' location (centred at $z \sim 1.5$ cm). Profiles are approximately Gaussian, and the area with vorticity ranges from -0.5 to 2.0 cm (roller 'core'). The area with core vorticity higher than $\sim 50\%$ of the peak is called the roller 'centre'; its diameter is ~ 1 cm at this stage, and it is denoted by a. The remainder is called the roller 'periphery'; it extends from the 'centre' to the region with no vorticity and at this stage has an outside diameter of ~ 2.5 cm and is ~ 0.75 cm thick (denoted by b). These two areas serve as a reference for the three-dimensional plots shown later in the paper.

taking place closer to the knife edge (a–c). Three-dimensional measurements will most effectively reveal the full shape of these structures.

Sections (y, z) through the centre of the pairing at the two locations (figure 7) display local three-dimensionality. As the two rollers continue to approach each other and pair, three zones are discerned in the vorticity field – an increasingly wavy periphery, a merging centre, and the section between these two zones. The processes in the centre are more vigorous than those in the outer regions because the centre points attempt to accommodate a new vorticity value (changing rapidly from the original peripheral value). Diffusion ultimately smooths the merged structure. The waviness on the periphery of the high-speed-side roller has a wavelength ranging from 1.25 cm (centre of the figures) to 1.70 cm (upper and lower areas in the figures) – a range of 0.4 to 0.57 times λ_0; this result is in good agreement with linear-theory predictions (Rogers & Moser 1993). Also, the centre of the core of the rollers and the merging zone exhibit a bulged nature and have a similar wavelength. The centre of the interaction (the new

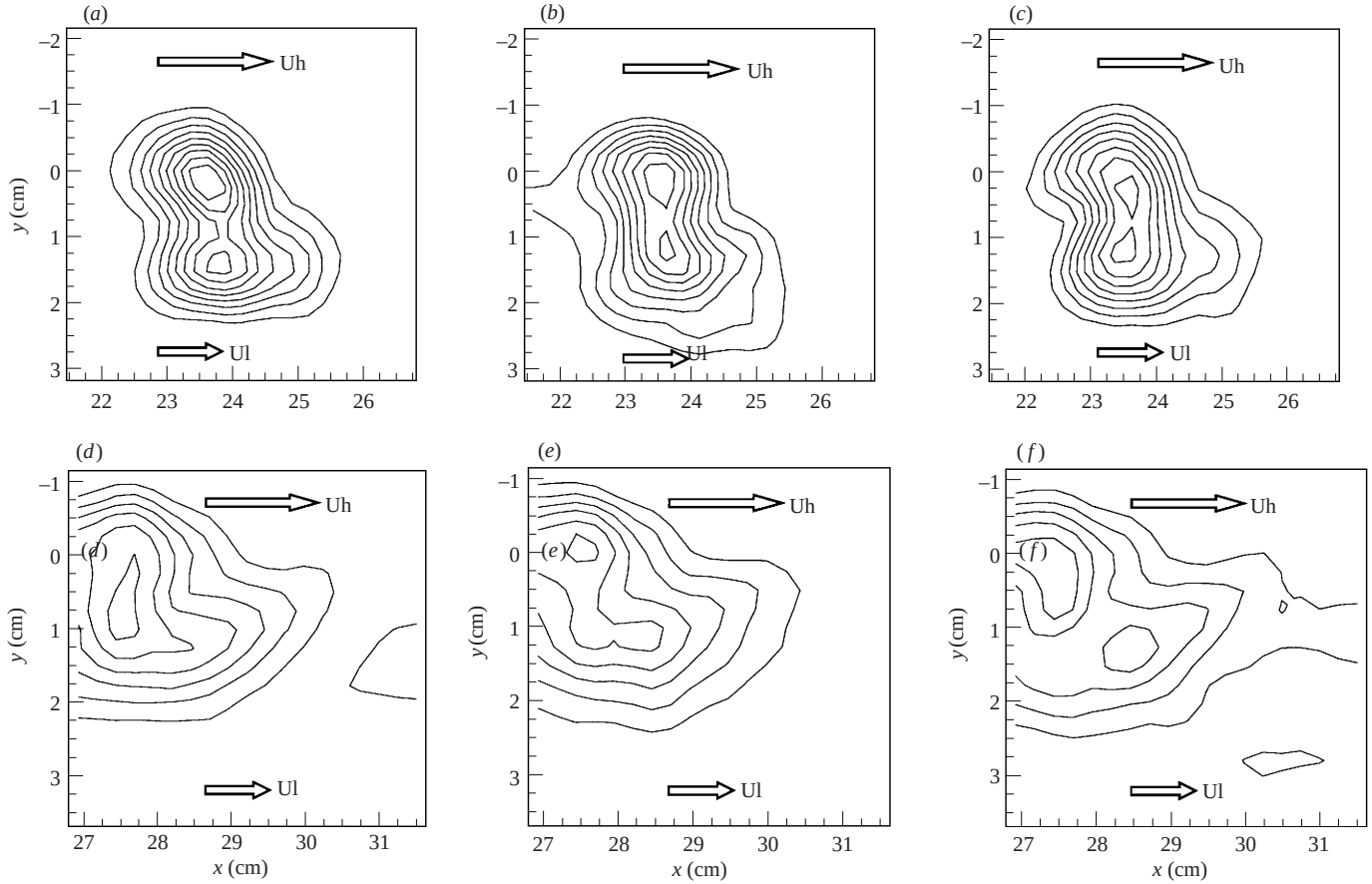

FIGURE 5. Sections (x, y) of two vortex-pairing locations: (a) $z = 0.25$ cm, (b) $z = 1$ cm, (c) $z = 1.5$ cm, (d) $z = -2.25$ cm, (e) $z = -1$ cm, (f) $z = 0.5$ cm (a–c: closer to knife edge; d–f: farther downstream), showing phase-averaged spanwise-vorticity variations. $\langle\omega_z\rangle = 75$ to 500 @ 50 s^{-1}. High-speed (Uh) and low-speed (Ul) sides indicated by arrows.

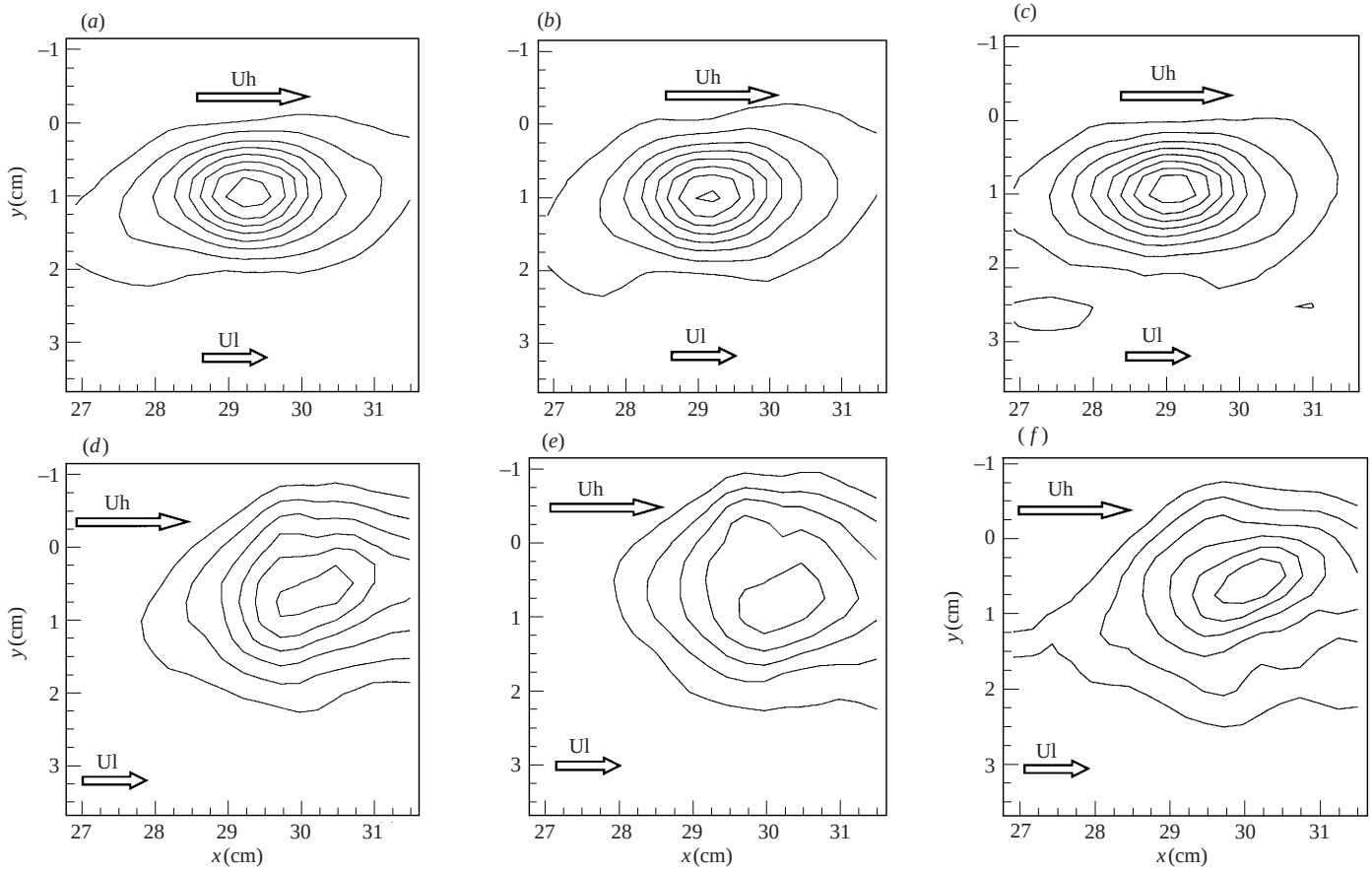

FIGURE 6. Sections (x, y) of merged structures for two pairing locations: (a) $z = -2.5$ cm, (b) $z = -1$ cm, (c) $z = 0.5$ cm, (d) $z = -2.5$ cm, (e) $z = -1$ cm, (f) $z = 0.5$ cm (a–c: closer to knife edge; d–f: farther downstream), showing phase-averaged spanwise vorticity. (a–c) $\langle\omega_z\rangle = 75$ to $800 \,@\, 75\,\mathrm{s}^{-1}$ (d–f) $\langle\omega_z\rangle = 75$ to $500 \,@\, 50\,\mathrm{s}^{-1}$. High-speed (Uh) and low-speed (Ul) sides indicated by arrows.

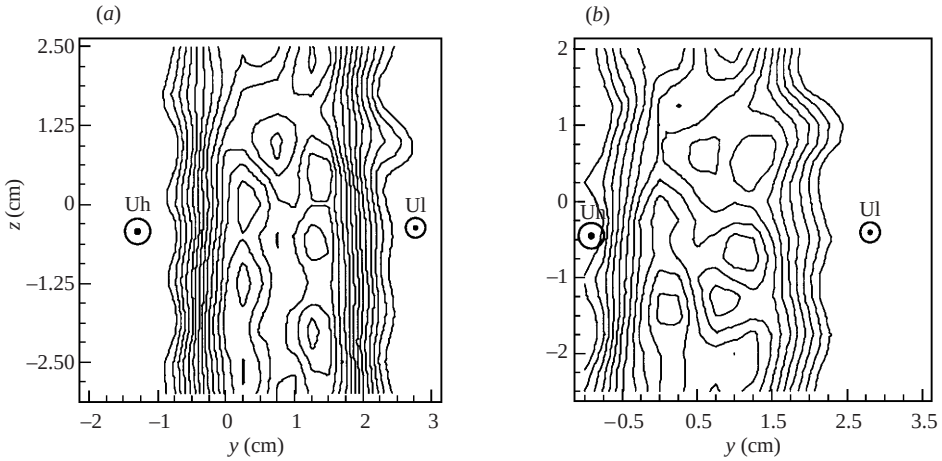

FIGURE 7. Sections (y, z) of phase-averaged spanwise vorticity during vortex pairing: (a) pairing closer to knife edge; section at $x = 23.5\,\text{cm}$; $\langle\omega_z\rangle = 70$ to $520 \,@\, 40\,\text{s}^{-1}$; (b) pairing farther downstream; section at $x = 27.75\,\text{cm}$; $\langle\omega_z\rangle = 70$ to $335 \,@\, 25\,\text{s}^{-1}$. High-speed (Uh) and low-speed (Ul) sides indicated.

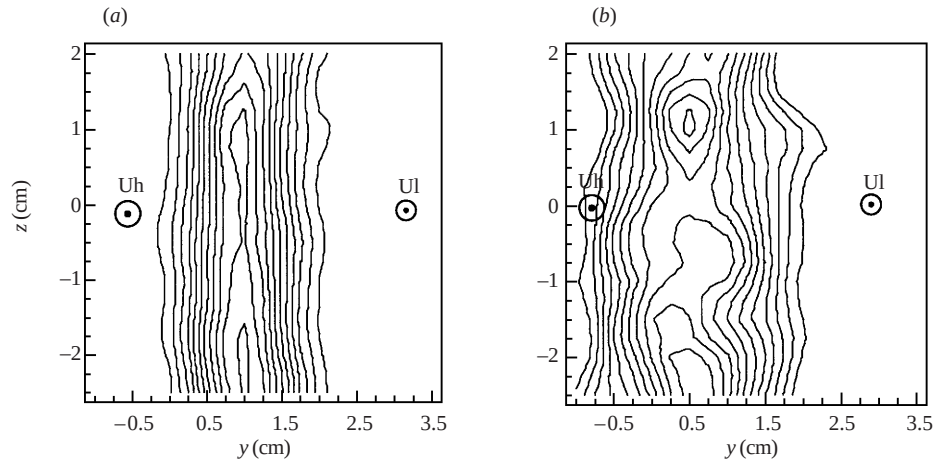

FIGURE 8. Sections (y, z) of phase-averaged spanwise vorticity of merging: (a) vortex merged closer to knife edge; section at $x = 29.25\,\text{cm}$; $\langle\omega_z\rangle = 70$ to $640 \,@\, 55\,\text{s}^{-1}$; (b) vortex merged farther downstream; section at $x = 29.50\,\text{cm}$; $\langle\omega_z\rangle = 100$ to $370 \,@\, 25\,\text{s}^{-1}$. High-speed (Uh) and low-speed (Ul) sides indicated.

centre of the merging structure) exhibits the strongest changes in vorticity – a sign of three-dimensionality, especially near the area of the largest upstream perturbation that produced a kink. The merged structure for the pairing that occurs closer to the knife edge appears to be quasi-two-dimensional (figure 8a). This is supported by the almost straight vorticity lines and the higher values of vorticity. The pairing that occurs farther downstream appears to be more disorganized, and evidence of non-axisymmetric three-dimensional modes (e.g. 'snake-like') in the farther downstream merging (figure 8b) will be presented though three-dimensional iso-surfaces.

Figure 9 displays the spanwise-vorticity profiles in the transverse direction for the pairing of figure 7(a) (shown interpolated in figure 9a) at eight (b) and twelve (c) equally spaced z- and y-locations, respectively. The peak values are lower near the

'kink' location (centred at $z = 1.5$ cm). The area with vorticity ranges from -1 to 3.0 cm (merging roller). The area with a core vorticity that is higher than $\sim 50\%$ of the peak (merging 'centre') has a diameter of ~ 2.5 cm at this stage and is denoted by a; the remainder ('periphery') extends from the 'centre' to the region with no vorticity; at this stage it has an outside diameter of ~ 4 cm and is ~ 1 cm thick (denoted by b). The roller is displayed as an interpolated image that emphasizes the two areas that serve as a reference for the slices from the three-dimensional plots shown later in the paper. The transverse profiles (figure 9*c*) display the phase relations of the spanwise waves. Both of the outermost sides of the periphery exhibit in-phase undulations as seen in figure 9(*a*). This translates to the opposite phases of the profiles captured in the constant y-sections, as shown in figure 9(*c*). The cores that exhibit bulges are out-of-phase with respect to each other and are shifted out-of-phase with respect to the periphery waves: the z-locations of their peaks (minima and maxima) correspond approximately to the z-locations of the valleys of the peripheral waves. The apparent tilting of the roller with respect to the z-axis accounts for the fact that the correspondence between the waves is also slightly tilted with respect to the z-axis.

These results support the fact that vortex pairing is spanwise non-uniform (but periodic) and occurs at different rates of progression in spanwise areas separated by the most amplified linear-theory wavelengths. While the crests of the nearly periodic spanwise wave have already merged, the valleys are still in the initial stages of pairing. Two modes are apparent – translative and bulging. Other modes (e.g. helical) can become amplified during first pairing if their energy is comparable to that of other instability modes, especially the strongest two-dimensional mode (first subharmonic). For instance, this can occur in a delayed pairing that takes place very far downstream where the two-dimensional rollers have sufficiently weakened. Since pairing rollers differ in strength and/or size, each roller is subject to a distinct instability amplification rate. Linear-theory instability analyses have explained the occurrence of the instability-mode amplification (Pierrehumbert & Widnall 1982; Moser & Rogers 1993; Schoppa *et al.* 1995) for equal-strength rollers. Spanwise-forcing experiments have been very successful in tracking the most amplified translative mode; however, mode amplification begins at the forcing location (splitter plate) and is always accompanied by 'ribs' (Lasheras *et al.* 1986). Experiments more similar to the linear-range analysis require a spanwise-unforced mixing layer, and evidence of instability-mode amplification has been reported (in experiments using Taylor's hypothesis) for the translative (Tung & Kleis 1996; Estevadeordal & Kleis 1999*a*), bulging (Estevadeordal & Kleis 1999*a*), and helical (Estevadeordal & Kleis 1999*b*) modes. In a smoke visualization study (Chandrsuda *et al.* 1978), helical pairing was reported but appeared to result from a strong local kink that amplified a non-axisymmetric mode beyond linear growth at a single location. Instability modes can be identified most effectively through three-dimensional measurements.

Figures 10–12 show the evolution of the roller core centres (labelled a) during pairing and merging. The detailed data clearly show that the rollers approaching each other (i) are quasi-two-dimensional (figure 10), (ii) become wavy as they pair (figure 11), (iii) pair through 'bridges' (transverse connections with spanwise vorticity between rollers) spanwise quasi-periodically (figure 11), and (iv) merge into a single structure which is either quasi-two-dimensional (figure 11) or less axisymmetric and corrugated (figure 12), depending on the pairing location. The structure from the farther downstream pairing displayed in figure 12 (*d–f*) has a 'snake'-like form. The wavelength of the non-axisymmetric wave (between 1 and 2 cm) is similar to that of the axisymmetric modes (translative and bulging), which are amplified in the

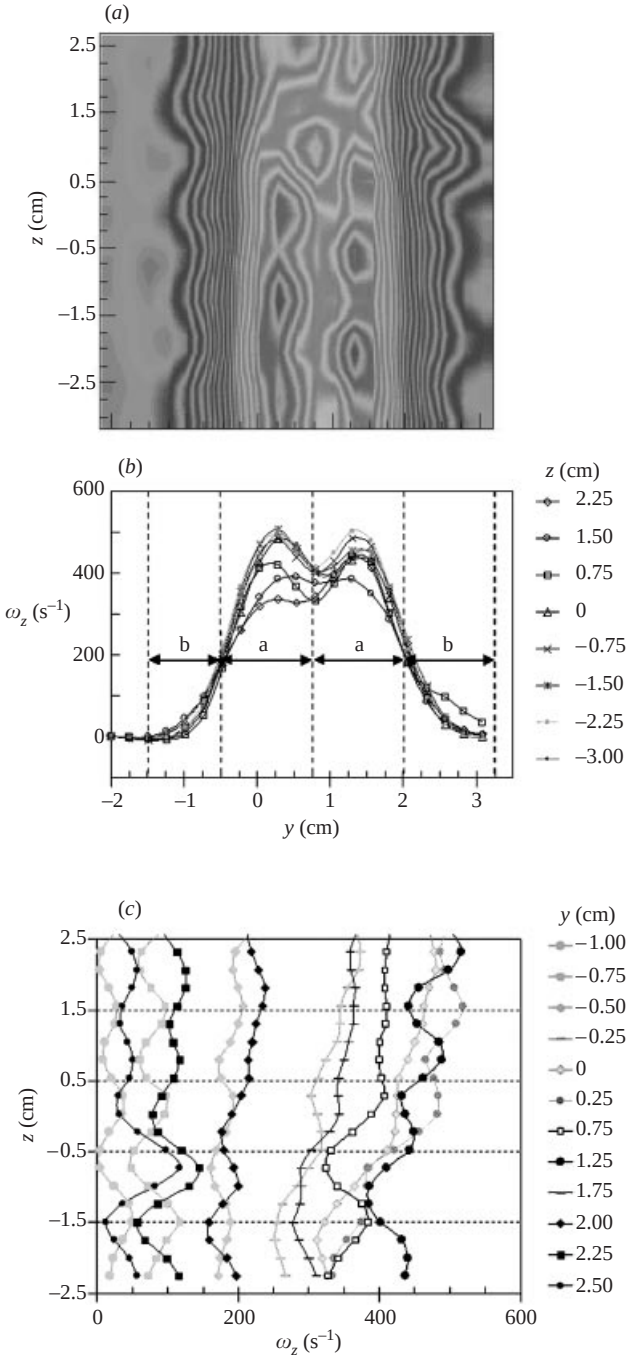

FIGURE 9. Spanwise-vorticity profiles in the transverse direction for vortex pairing of figure 7(*a*) (shown interpolated in (*a*) at eight (*b*) and twelve (*c*) equally spaced *z*- and *y*-locations, respectively. Lower peak values occur near the 'kink' location (centred at $z = 1.5$ cm). The area with vorticity ranges from -1 to 3.0 cm (merging roller). The area with core vorticity higher than $\sim 50\%$ of peak (merging centre) has average diameter of ~ 2.5 cm at this stage and is indicated by *a*; the remainder ('periphery') extends from the center to the region with no vorticity and at this stage has outside average diameter of ~ 4 cm and average thickness ~ 1 cm (indicated by *b*). The roller is shown as an interpolated image, emphasizing the two areas which serve as a reference for the slices from the three-dimensional plots shown later in the paper.

farther upstream pairing location. Amplification of the non-axisymmetric mode can result from the co-existence of axisymmetric and helical modes in farther downstream pairing locations and give the structure a 'snake'-like form.

Assessment of the duration or persistence of two-dimensionality for independent rollers (without pairing) is under study. Changing the phase of, for instance, the first subharmonic wave to produce shredding will allow assessment of the distance which the solitary rollers can travel without becoming three-dimensional. The present results support the fact that under ideal conditions (meaning absence of perturbations), two identical two-dimensional rollers can pair spanwise uniformly. However, slight perturbations (e.g. local defects) trigger three-dimensional motions that become further amplified by mutual and self-induced motions. Through the pairing interaction the rollers lose their two-dimensionality as they approach each other and, at a downstream location where they are two-dimensional before pairing, they acquire spanwise waviness (especially the low-speed-side roller) and pair through the crests of their waves forming bridges (Estevadeordal & Kleis 1999*a*). The spanwise periodicity has a wavelength of $\sim 0.6\lambda_0$. This wavelength also persists through the pairing process. The correspondence of minima and maxima of the waves from the periphery and centre of the rollers is shown in figure 13 for the pairing that occurs closer to the knife edge. In the centre of the pairing, the roller centres are initially out-of-phase (figure 13*b*). At the end the merging roller (figure 13*f*) still has a centre bulged structure. Figure 14 presents evidence of axial velocities consistent with bulged rollers during pairing. These velocities are not as high as those reported in other studies (Schoppa *et al.* 1995), but a direct comparison between the two studies has not been made.

It is noteworthy that the initial forcing conditions control the location of the pairing and, in turn, its three-dimensional characteristics. Forcing, which includes the second subharmonic, generates two pairing locations and two consecutive merged structures with peculiar three-dimensionality. A schematic of first roller pairings, based on the spanwise-vorticity results, is shown in figure 15 for two downstream pairing locations. It should be noted that the relative phasing of the spanwise waves is altered by the pairing. Initially the waves of both rollers are in-phase (as in the translative modes illustrated in figure 9 of Pierrehumbert & Widnall 1982) and become out-of-phase (similar to the helical modes illustrated in figure 6 of Pierrehumbert & Widnall 1982) as they pair and merge locally; the present results show that a change in relative phase occurs and suggest that more than one instability mode develops simultaneously. Applying three-dimensional perturbations to a periodic row of vortices, Pierrehumbert & Widnall (1982) found two main instability modes that involve spanwise core (planar) variations – the aforementioned translative mode and the helical mode. The translative instability (sinusoidal spanwise translation on the rollers) has a growth rate only slightly lower than that of the two-dimensional pairing, and it is often observed; the helical pairing (local twisting of the rollers around each other) is much less vigorous (lower growth rate) than the two-dimensional pairing and, thus, is often overridden and seldom observed. Pierrehumbert & Widnall (1982) studied other instability modes (such as bulging), but these exhibited less growth than the previous two. They suggested the possibility of physical counterparts to some of the higher-order modes that involve smaller scales, such as short-wave instabilities. A study by Schoppa *et al.* (1995) revealed that the bulging mode can exhibit faster growth than the others, depending on the initial conditions. Since the core instabilities depend on the initial conditions and core size and shape, in a practical situation where the rollers are different (e.g. the low-speed side is 'weaker', as explained earlier), these

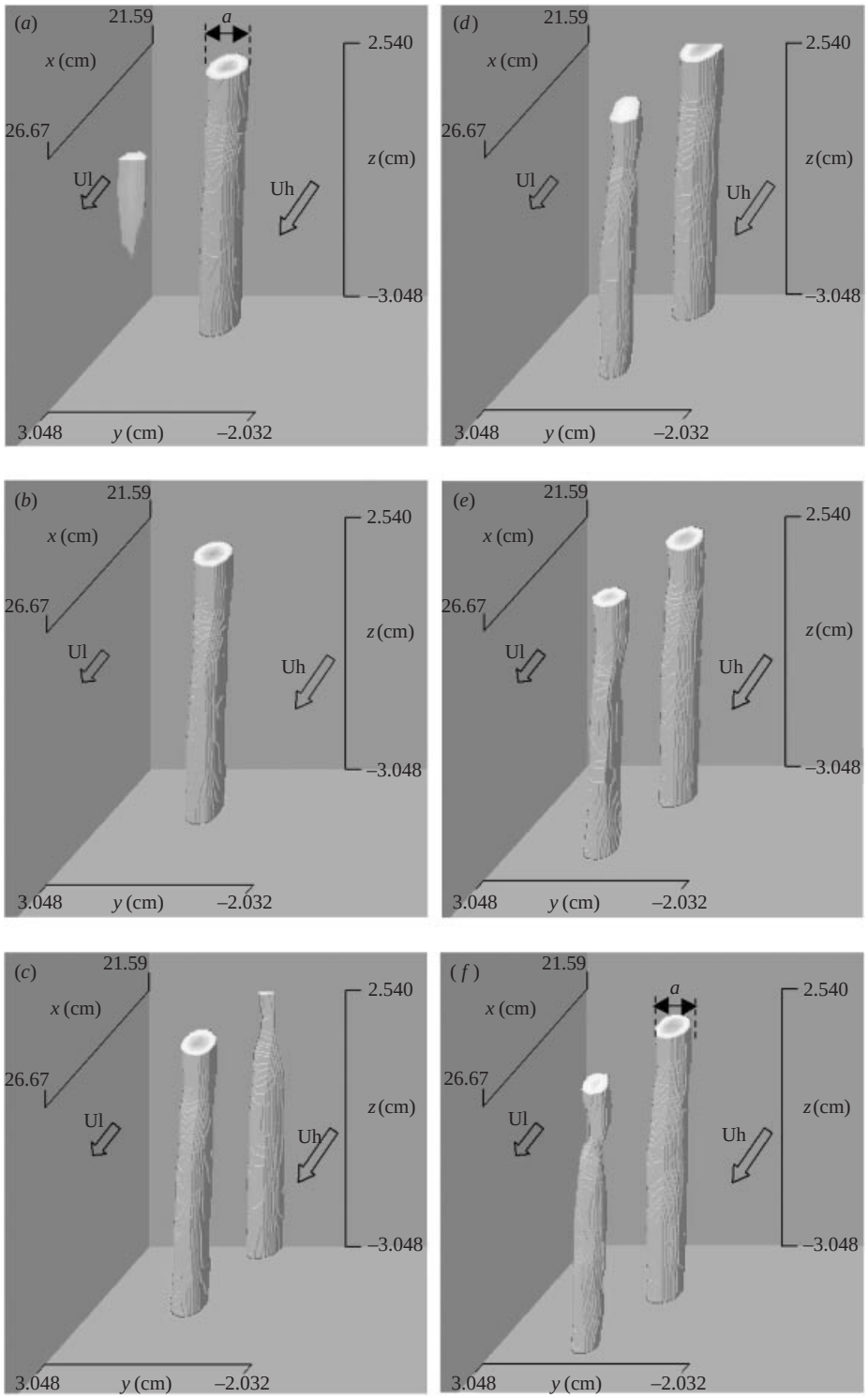

FIGURE 10. Rollers through the first grid. Iso-surfaces of phase-averaged spanwise vorticity for roller centres a ($\langle\omega_z\rangle = 400\,\mathrm{s}^{-1}$) for six phases of the second-subharmonic cycle. High-speed (Uh) and low-speed (Ul) sides indicated by arrows. (a) Phase 0, (b) phase 1, (c) phase 2, (d) phase 3, (e) phase 4, (f) phase 5.

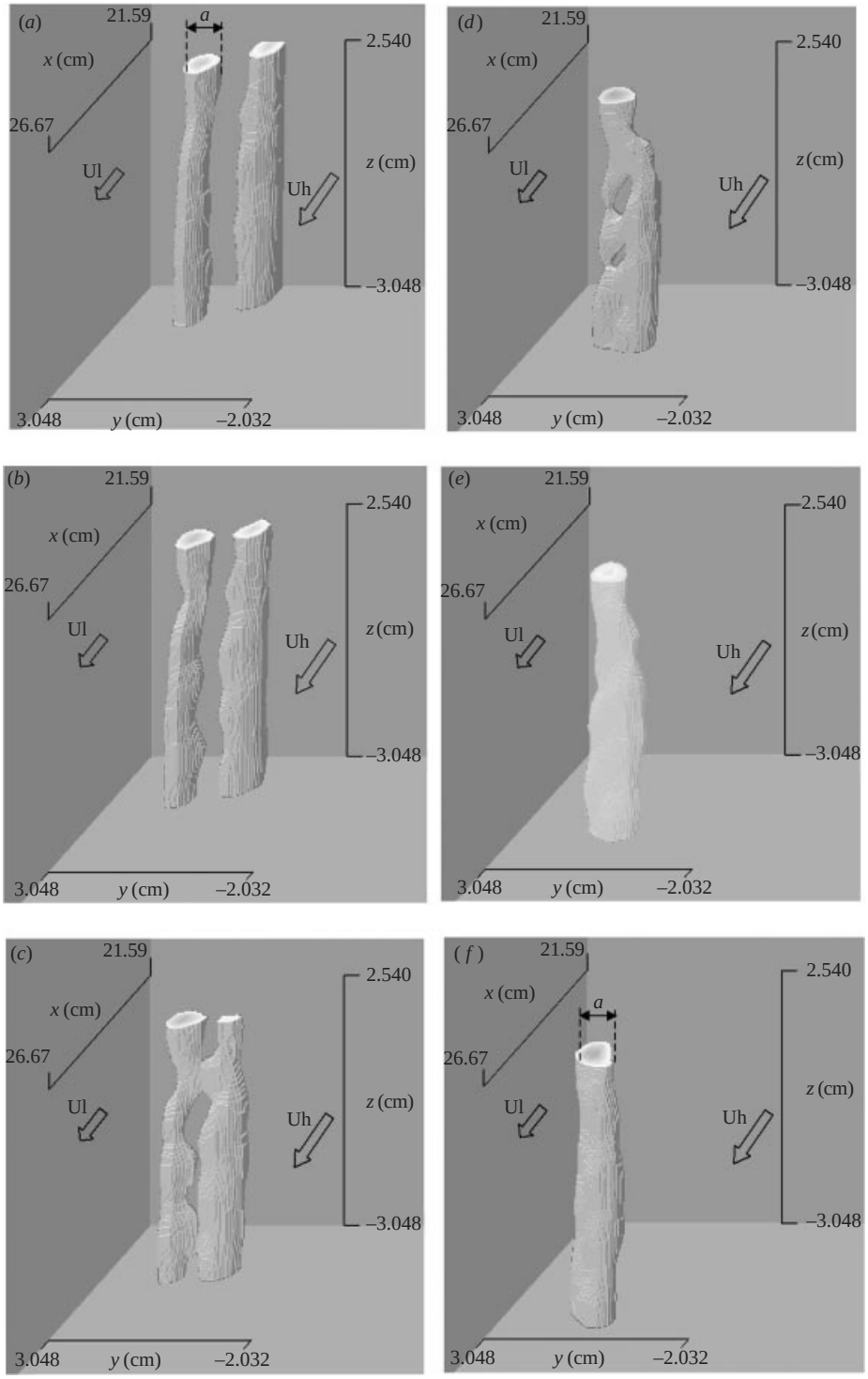

FIGURE 11. Evolution of roller centres a through pairing at first grid. Iso-surfaces of phase-averaged spanwise vorticity ($\langle\omega_z\rangle = 400\,\mathrm{s}^{-1}$) for six phases of the second-subharmonic cycle. High-speed (Uh) and low-speed (Ul) sides indicated by arrows. (*a*) Phase 12, (*b*) phase 13, (*c*) phase 14, (*d*) phase 15, (*e*) phase 16, (*f*) phase 17.

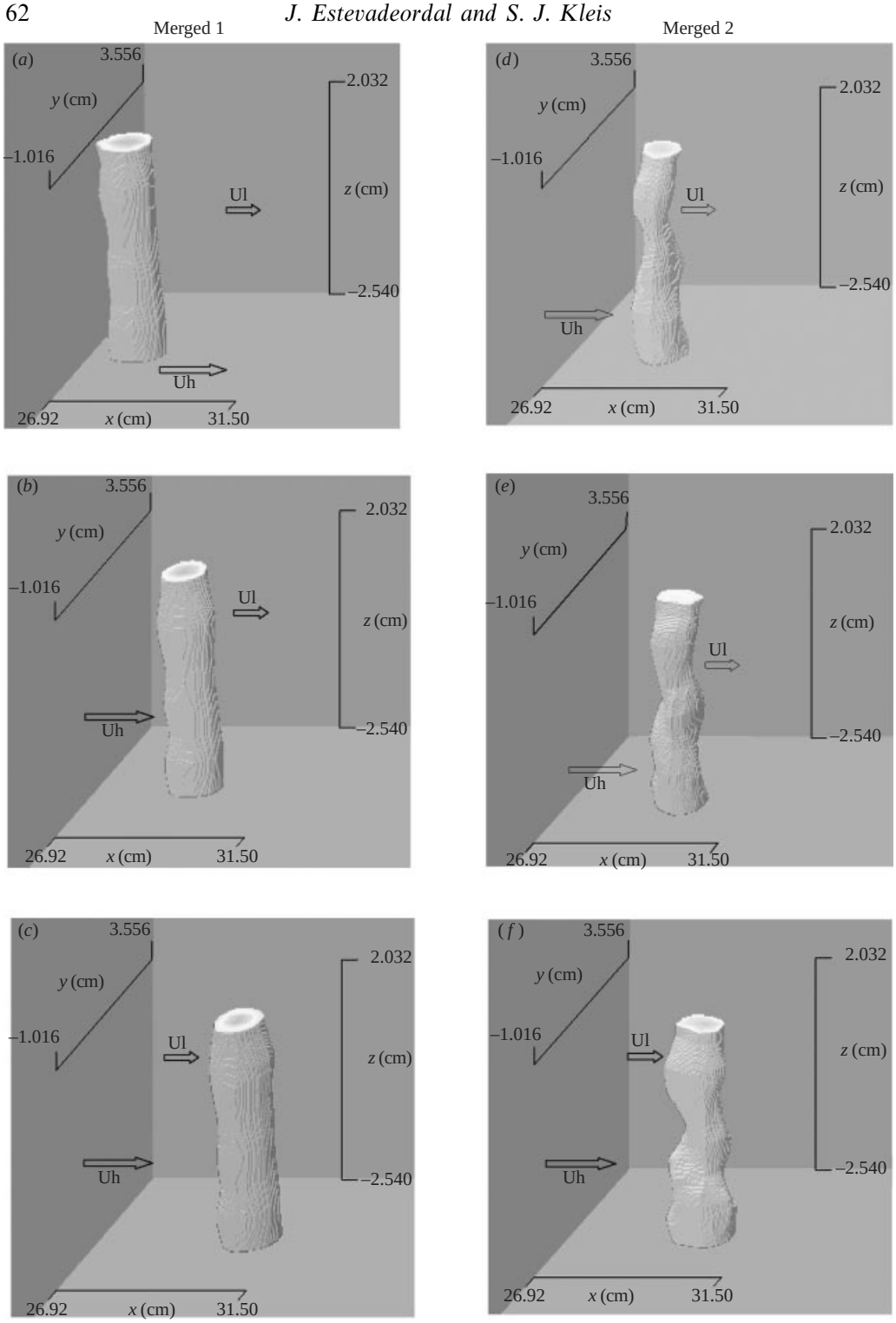

FIGURE 12. Comparison of merged rollers. Iso-surfaces of phase-averaged spanwise vorticity for a vortex that merged closer to knife edge ('Merged 1', *a–c*, $\langle\omega_z\rangle = 450\,\mathrm{s}^{-1}$) and for a vortex merged farther downstream ('Merged 2', *d–f* $\langle\omega_z\rangle = 270\,\mathrm{s}^{-1}$). High-speed (Uh) and low-speed (Ul) sides indicated by arrows. (*a*) Phase 1, (*b*) phase 3, (*c*) phase 5, (*d*) phase 12, (*e*) phase 13, (*f*) phase 14.

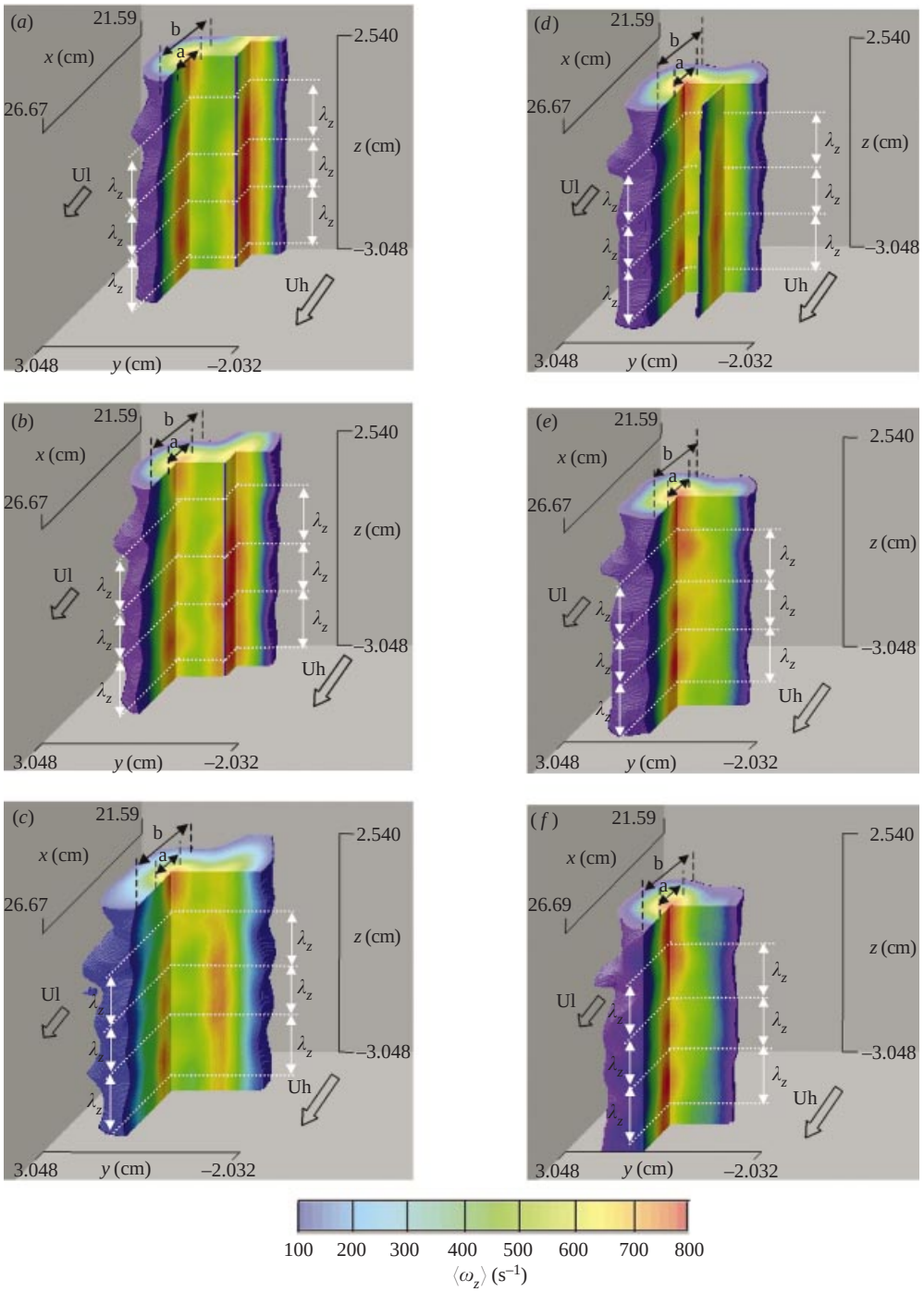

FIGURE 13. Roller-core evolution and relative spanwise-wave out-of-phasing between centre and periphery during pairing through the first grid. Iso-surfaces of phase-averaged spanwise vorticity ($\langle\omega_z\rangle = 100$ to $800\,\mathrm{s}^{-1}$) for six phases of the second-subharmonic cycle of figure 11. '*a*', '*b*', λ_0 and λ_z indicate centre, periphery, and streamwise and spanwise wavelengths, respectively. $\lambda_z \sim 0.5\lambda_0$.

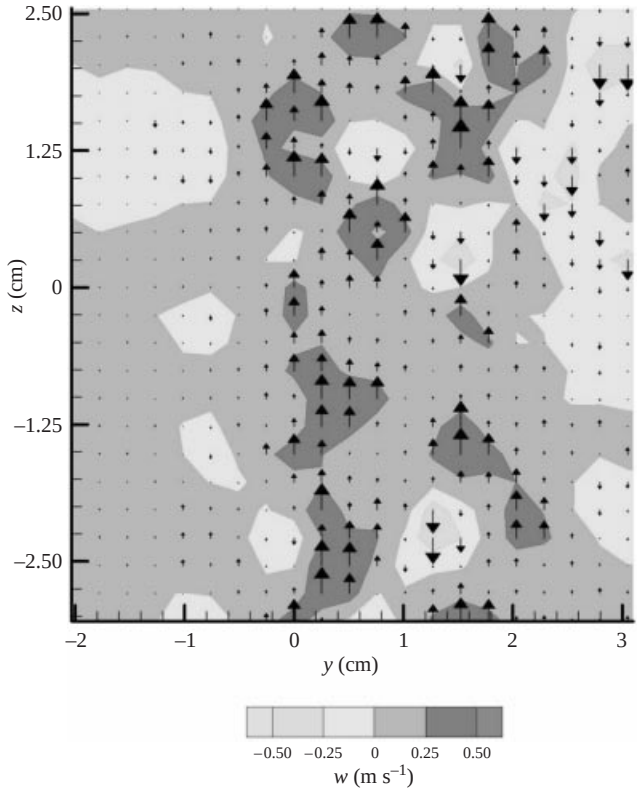

FIGURE 14. Section (y, z) of the phase average of the z-component of velocity (w) during vortex pairing (corresponding to figure 7a).

modes can initially grow and coexist before being overridden, for instance, by the strongest two-dimensional pairing. In addition, the secondary structures can play an important role (see the next section). The present results suggest that the change from in-phase to out-of-phase of the waviness of the rollers is due to the coexistence of at least two secondary instabilities. An instability mode different from the translative mode and similar to bulging is amplified on the rollers just after the translative mode develops; its effect on the low-speed-side roller is more dramatic. Since the low-speed-side roller is weaker (less vigorous coherent motion), it does not have sufficient stability to remain two-dimensional, especially farther downstream; the three-dimensionality is inhibited through pairing with the stronger high-speed-side roller. For first pairings that occur farther downstream, a third mode (non-axisymmetric) is also amplified, its nature and wavelength being consistent with short-wavelength instabilities and helical modes.

These roller instabilities appear to dictate the evolution of the mixing layer toward the onset of three-dimensionality and turbulence. The evolution and influence of the next important flow structures (the secondary structures) will now be discussed.

3.2. *Secondary structures*

The present study on vortex pairing revealed a number of counter-rotating pairs of secondary structures that are consistent with the linear-instability wavelength. In their streamwise-vorticity-evolution study, Tung & Kleis (1996) suggested that the secondary structures are generated during pairing, simultaneously with the spanwise

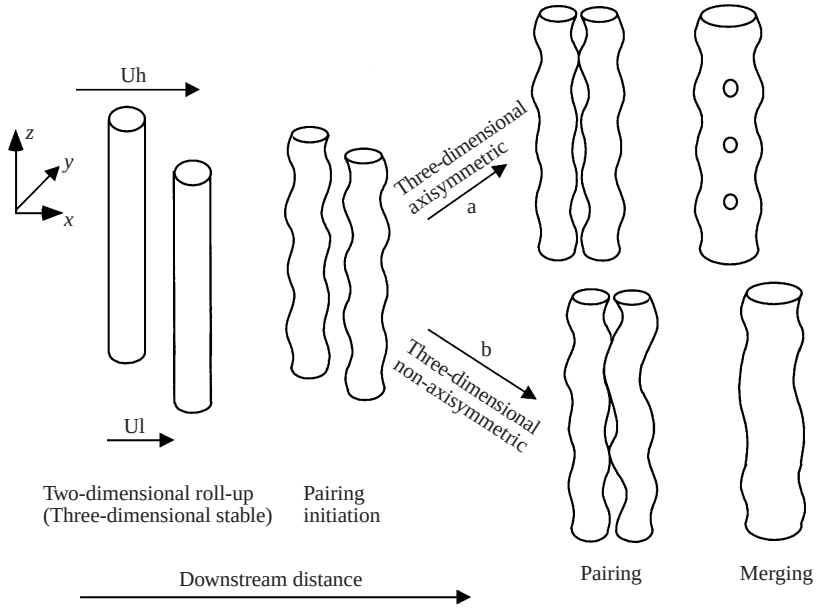

FIGURE 15. Schematic of the effect of the downstream location of first pairing on the amplification of instability modes: (*a*) pairing closer to knife edge, with rollers preserving axisymmetry; (*b*) pairing farther downstream, with amplification of non-axisymmetric modes. Lines represent iso-vorticity values. Uh is high-speed and Ul is low-speed.

instability on the rollers. They found that only localized patches of streamwise vorticity having low values (<10% of the spanwise vorticity) exist before pairing and that these patches are not yet organized into secondary structures. These areas were associated with the upstream perturbations that produced kinks on the rollers.

The present three-dimensional measurements provide new information regarding the independence of these secondary structures, how they are affected by the rollers, their influence on roller instabilities, their physical connection with the rollers, and how the structures on the shrinking braid disappear between the pairing rollers.

Figure 16 shows the characteristic forms (Metcalfe *et al.* 1987; Rogers & Moser 1992; Tung & Kleis 1996) of the secondary structures educed from the present measurements. The (x, y) cuts through the centre of the secondary structures (figure 16*a*, *b*) display the typical layered pattern of the streamwise vorticity across the mixing layer (five layers alternating in sign, with continuous lines and dashed lines representing positive and negative values of streamwise vorticity, respectively). The streamwise vorticity at the location corresponding to the spanwise rollers has sign opposite that of the secondary structures that wrap around them (figure 17*a*). This means that the rollers are tilted in alternate fashion; the streamwise vorticity of the rollers is much weaker than that of the secondary structures. The values of streamwise vorticity of the secondary structures are much lower than those of the spanwise vorticity of the rollers, the maximum value being about 10 times lower, and the minimum value (that of the outer contour) being near zero. Primary and secondary structures appear connected by their weakest vorticity values, suggesting (at least from these phase-averaged measurements) that they are not strongly connected at this stage. Nevertheless, the fact that they have the same spanwise wavelength implies that the same small perturbations are responsible for the generation of both the roller waves and the secondary structures.

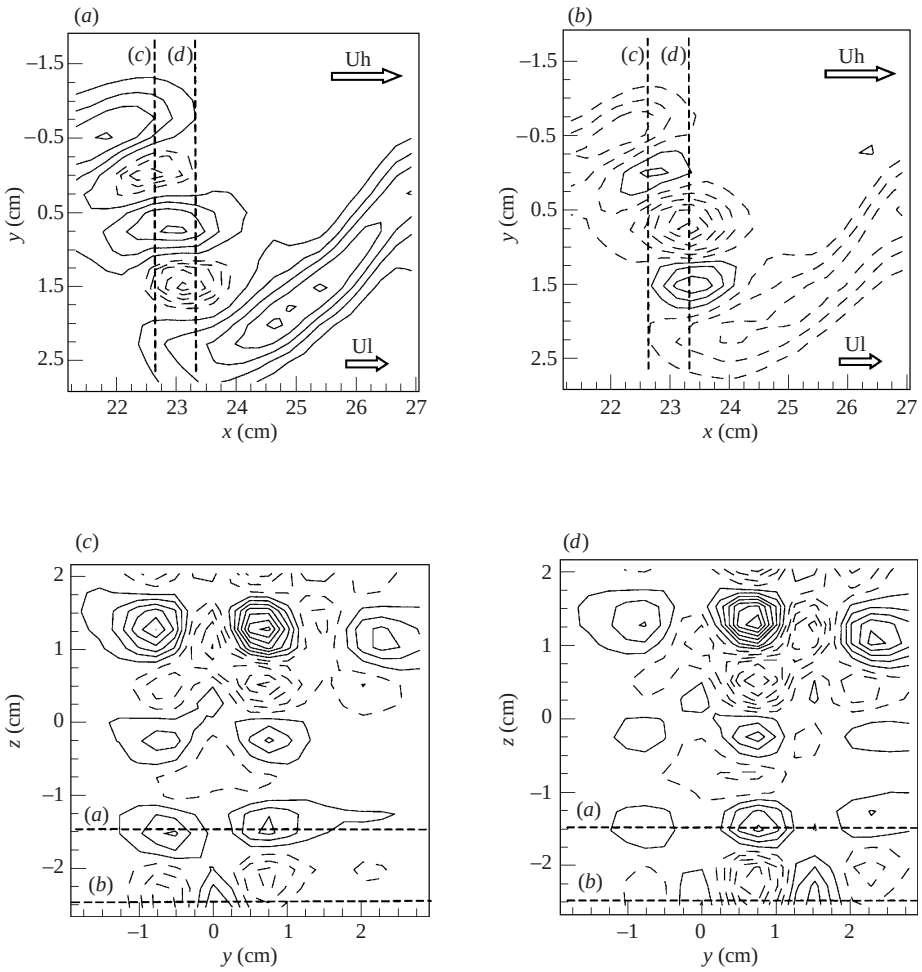

FIGURE 16. Secondary structures at first pairing. Iso-contours of the phase-averaged streamwise vorticity ($\langle\omega_x\rangle\,\mathrm{s}^{-1}$): (*a*) ($x$, y)-plane at $z = -1.524\,\mathrm{cm}$, (*b*) (x, y)-plane at $z = -2.54\,\mathrm{cm}$, (*c*) (y, z)-plane at $x = 22.6\,\mathrm{cm}$, (*d*) (y, z)-plane at $x = 23.36\,\mathrm{cm}$. Dashed contours are $\langle\omega_x\rangle = -150$ to $0 \,@\, 25\,\mathrm{s}^{-1}$; continuous contours are: (*a*) $\langle\omega_x\rangle = 35$ to $225 \,@\, 45\,\mathrm{s}^{-1}$, (*b*) $\langle\omega_x\rangle = 0$ to $75 \,@\, 25\,\mathrm{s}^{-1}$, (*c*, *d*), $\langle\omega_x\rangle = 0$ to $160 \,@\, 25\,\mathrm{s}^{-1}$. High-speed (Uh) and low-speed (Ul) sides indicated. Sections indicated by dashed lines.

The (y, z) cuts normal to the flow (figure 16*c*, *d*) exhibit 'quadrupole' configurations (Rogers & Moser 1993) formed by structures of different strengths. The planes shown are cuts through the cores of the pairing rollers and form a set of five columns. The strongest structures are located near the area where the rollers have the noticeable kink (figure 17*b*). It was pointed out previously that as the rollers approach each other, a wavy pattern is generated in both their periphery and their core that is consistent with the quadrupole configuration (figure 18). The downstream evolution of this configuration depends on the strength and induced fields of the different structures that generate the 'mini' mixing layers shown schematically (only the vertical flow pattern is shown for simplicity) in figure 18(*b*).

The column of secondary structures between the pairing rollers is a part of the shrinking braid, which is being compressed in the middle. This braid disappears once merging is complete. The streamwise vorticity in this braid is patchy and is a source

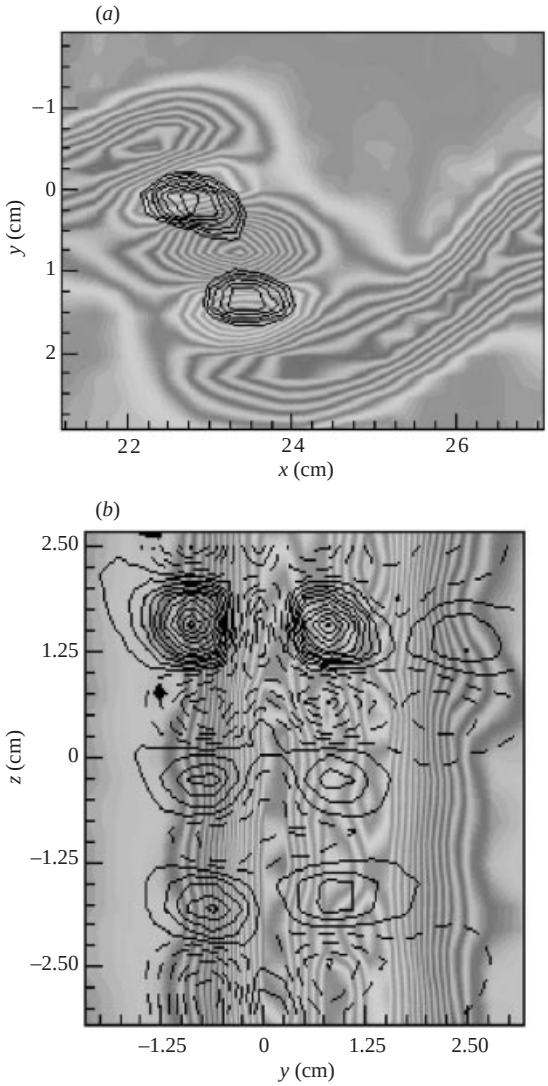

FIGURE 17. Relative position of rollers and secondary structures. (*a*) Iso-contours of phase-averaged spanwise vorticity of rollers over the interpolated image of streamwise vorticity of figure 16(*a*). (*b*) Iso-contours of phase-averaged streamwise vorticity of figure 16(*c*) over interpolated image of spanwise vorticity of figure 7(*a*).

of phase-random three-dimensionality during pairing (Tung & Kleis 1996). The roller waves and alternating-vorticity sign in the quadrupole configuration suggest that the secondary structures of the shrinking braid disappear into the rollers through tearing. It should be noted that the inner three-dimensionality of the merging process (e.g. secondary-structure motion in the shrinking braid) is greatly inhibited by the pairing rollers that generate a quasi-two-dimensional structure with mainly spanwise vorticity.

The relation of the peripheral wave to the secondary structures of the braid was displayed by superimposing the streamwise-vorticity contours and the interpolated image of the spanwise vorticity in figure 17(*b*). Each pair of counter-rotating secondary structures resides in a valley of the roller wave, especially in the area far from the kink.

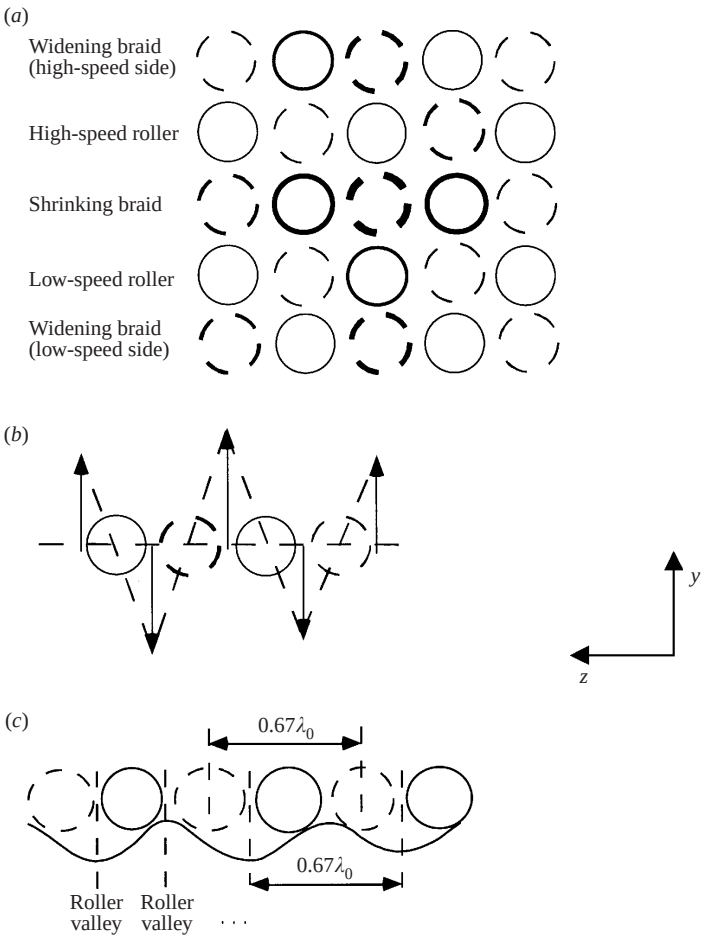

FIGURE 18. (*a*) Schematic of secondary-vorticity 'quadrupole' configuration (cut normal to the streamwise direction through the middle of initial pairing rollers); (*b*) vertical induced flow patterns; (*c*) schematic of relative position of rollers and secondary structures. Wavy line corresponds to periphery of rollers, and circles correspond to secondary structures. Theoretical spacing is $0.67\lambda_0$. Solid and dashed lines indicate opposite signs, and line thickness indicates different strengths.

Each pair is separated from the next by the crest of the peripheral wave. Thus, the distance between counter-rotating secondary-vortex pairs corresponds to the spanwise wavelength of the rollers (shown schematically in figure 18*c*). The correspondence between quasi-periodic bridging and streamwise structures indicates that these features are manifestations of the same three-dimensional instability. This configuration shows that the areas corresponding to the bridges (where the first contact between pairing rollers occurs) are three-dimensional, having noticeable spanwise and streamwise vorticity components. These areas do not correspond to the initial streamwise patches of the shrinking braid because the initial waves of the rollers are in phase. Thus, complex three-dimensional events are occurring that involve the induced motion (figure 18*b*) and the simultaneous growth and decay of several instabilities (such as those reported for the rollers), which result in tearing of the secondary structures upon merging. The secondary structures of the widening braid persist and become elongated. From the present data it is possible to estimate their size and shape. They

are inclined with respect to the streamwise direction, forming an angle of about 30° at this pairing location and, thus, project a vorticity component onto the y-direction. For this reason the term secondary structure is preferable to streamwise structure. Their length is ~ 5 cm at this location and is obviously dependent on the streamwise wavelength (which is being doubled).

The above results were corroborated by reconstructing the streamwise vorticity in longer spanwise domains. For capturing the first pairing, time series were obtained on the two-dimensional slice normal to the streamwise direction located at $x = 22.86$ cm. It should be noted that the streamwise vorticity in a (y, z)-plane computed from those time series does not require any assumption (such as Taylor's hypothesis) since the streamwise-vorticity component does not involve a streamwise derivative. The results were also used to determine the characteristics (strength and circulation) of the secondary structures that allow a practical measurement of the collapse parameter (Lin & Corcos 1984).

Pairs of counter-rotating secondary structures in the (y, z)-plane that cuts through the cores of the rollers are shown in figure 19(a). Again, the braid is organized in straight rows and columns, emphasizing its rectangular quadrupole configuration. The centres of the secondary structures can be joined in straight lines in any direction. Along these lines the secondary structures are of alternate sign, and every secondary structure is surrounded by structures of the opposite sign. The most prominent structures are those in the area of the kink. Figure 19(b) is a line plot of the streamwise vorticity in the cut as a function of spanwise distance and shows that for the strongest pair the positive value of streamwise vorticity is higher than the negative. This asymmetry is determined by the evolution of the flow from the largest upstream perturbation. The plot also shows that the strength is similar in the other structures in the row.

For measuring the strength and collapse parameter of the secondary structures, the circulation is computed by integration of the vorticity values over the area of a selected vortex. The boundary is carefully selected from the data in such a way that no negative values are inserted into a positive vortex and vice versa. For this particular vortex, the circulation is $0.0160\ \mathrm{m^2\ s^{-1}}$; normalized, this value is 0.0016. The normalization is the same as that for the spanwise circulation, i.e. normalized by the product of (i) the initial maximum spanwise vorticity, $(\partial U/\partial y)_{max}$, (ii) the sum of the high and low boundary-layer momentum thickness, $\theta_H + \theta_L$, and (iii) the fundamental wavelength, λ_0:

$$\Gamma_x^* = \frac{\Gamma_x}{(\partial U/\partial y)_{max}(\theta_H + \theta_L)\lambda_0}, \tag{3.1}$$

where Γ_x^* is the normalized value of the circulation Γ_x and the subscript indicates the plane in which the curve lies. The circulation of the secondary structures (by the braid) computed using this method is shown in figure 19(c).

The secondary structures are approximately of circular cross-section, and their formation can be understood through the collapse mechanism explained by Lin & Corcos (1984). Their criterion establishes a critical parameter based on strain and circulation, above which the braid always collapses into compact, nearly axisymmetric vortices. In fact, the value of the critical parameter is sufficiently low for the braid to collapse into nearly circular secondary structures under most circumstances. This condition is more pronounced when a kink is present and also during a strong interaction such as pairing (spanwise unstable to small perturbations, as shown previously). An estimate of the collapse parameter ($\mathscr{L}$) is given in Rogers & Moser

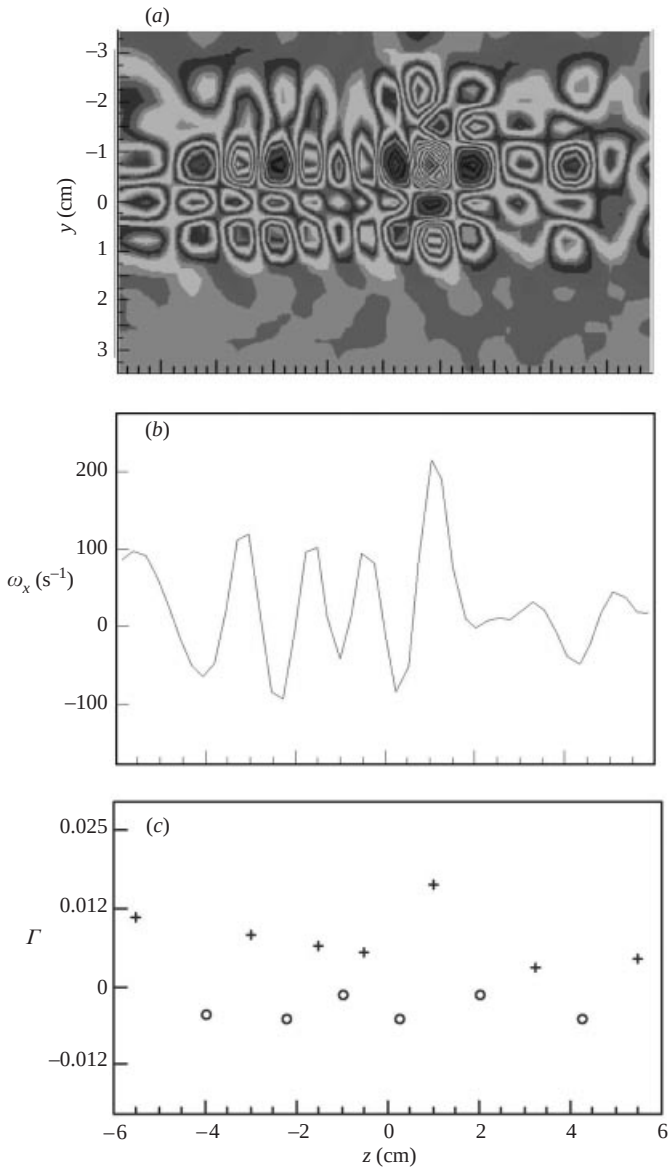

FIGURE 19. (*a*) Streamwise vorticity at first pairing ($x = 22.86$ cm) in (y, z)-plane through centre of pairing rollers; $\langle\omega_x\rangle = -550$ to $-40\,\mathrm{s}^{-1}$ (dark) and 47 to $750\,\mathrm{s}^{-1}$ (light). (*b*) Streamwise vorticity along $y = 0.75$ cm (of *a*); (*c*) Streamwise circulation (m^2 s^{-1}) (of *a*): +, positive; (○), negative.

(1992) as

$$\mathscr{L} = \frac{\Gamma_{rib}}{(S\lambda_z^2)^{1-p}\nu^p} > 13.1, \tag{3.2}$$

where $p = 0.6825$ is a curve-fit parameter from Lin & Corcos (1984), S is the maximum two-dimensional principal strain rate in the centre of the braid (in z), λ_z is the spanwise wavelength, and ν is the viscosity. The probability for collapse increases primarily with rib circulation and secondarily with Reynolds number and decreases primarily with spanwise wavelength and secondarily with strain rate. For a secondary

structure with 0.01 circulation, the estimated value of the parameter would be

$$\mathscr{L} = \frac{0.01}{(1000 \times 0.016^2)^{1-0.6825}(1.5 \times 10^{-5})^{0.6828}} \sim 30, \tag{3.3}$$

which is well above the critical value of 13.1; thus, we may assume that 'ribs' have collapsed into compact axisymmetric structures. From figure 19(*c*) it is obvious that the circulation values may be even lower than 0.01, in which case the collapse parameter would be even closer to the computational predictions. The compact and axisymmetric secondary structures shown in both the (x, y) and the (y, z) sections are very similar to those from numerical simulations (Metcalfe *et al.* 1987; Moser & Rogers 1993) and experiments using Taylor's hypothesis (Tung & Kleis 1996).

Time evolution of streamwise vorticity is displayed in the three-dimensional iso-surface plots of figures 20 and 21. The set of frames in figure 20 corresponds to the frames of figure 11 (the initiation of pairing in the first grid), and the ones in figure 21 correspond to those figure 12 (the passage of the merged structure in the second grid). In the first set (figure 20), shown in the same view as the rollers, the widening (or surviving) braid reveals prominent counter-rotating secondary structures (positive indicated as a–i). These structures move in the transverse direction as they follow the revolving motion of the pairing rollers. The structures are being elongated to approximately twice the fundamental wavelength, as can be inferred from the right-hand edge of the figures (the high-speed side), which shows that the length of the structures is at least that of the domain (about two fundamental wavelengths). The shrinking braid contains remnants of the secondary structures that are being compressed (positive indicated as *d*, *e*, *f*) and shows prominent connections near the area of the kink (a larger negative-streamwise-vorticity region near the positive indicated by *d*). From the first frame (phase 12) to the last (phase 17), these shrinking structures evolve from initially secondary structures to a patchy form as they are compressed into the spanwise merging structure. In the second set (figure 21), neatly arranged secondary structures associated with the passage of the quasi-two-dimensional merged spanwise structure (merged 1: frames *a–c*) cross the domain. As the new structures enter the domain near the high-speed side, the older ones in the domain travel toward the low-speed side, carried by the pairing rollers as they revolve around each other. These features occur in a more disorganized manner (less organized vorticity in the braid) in frames (*d–f*) (merged 2), which correspond to the more three-dimensional flow of the pairing that is occurring farther downstream. In all cases the evolution shows that the secondary structures do not move in the spanwise direction (no meandering), as reported by LeBoeuf & Mehta (1993).

4. Concluding remarks

Detailed three-dimensional measurements on vortex pairing in a large plane mixing layer revealed novel spanwise characteristics. It was found that the two rollers develop wavy peripheries as they approach each other and that pairing begins at the crests of the waves through a change in the relative phase between the waves of each roller. The spanwise waves were quasi-periodic, with a wavelength approximately between one-half and one fundamental streamwise wavelength; this corresponds to the most amplified perturbation waves predicted by linear theory (Pierrehumbert & Widnall 1982; Rogers & Moser 1993; Schoppa *et al.* 1995).

The spanwise rollers appear to be most susceptible first to the translative instability. The waviness is initially restricted to the periphery, is in-phase for the pairing rollers,

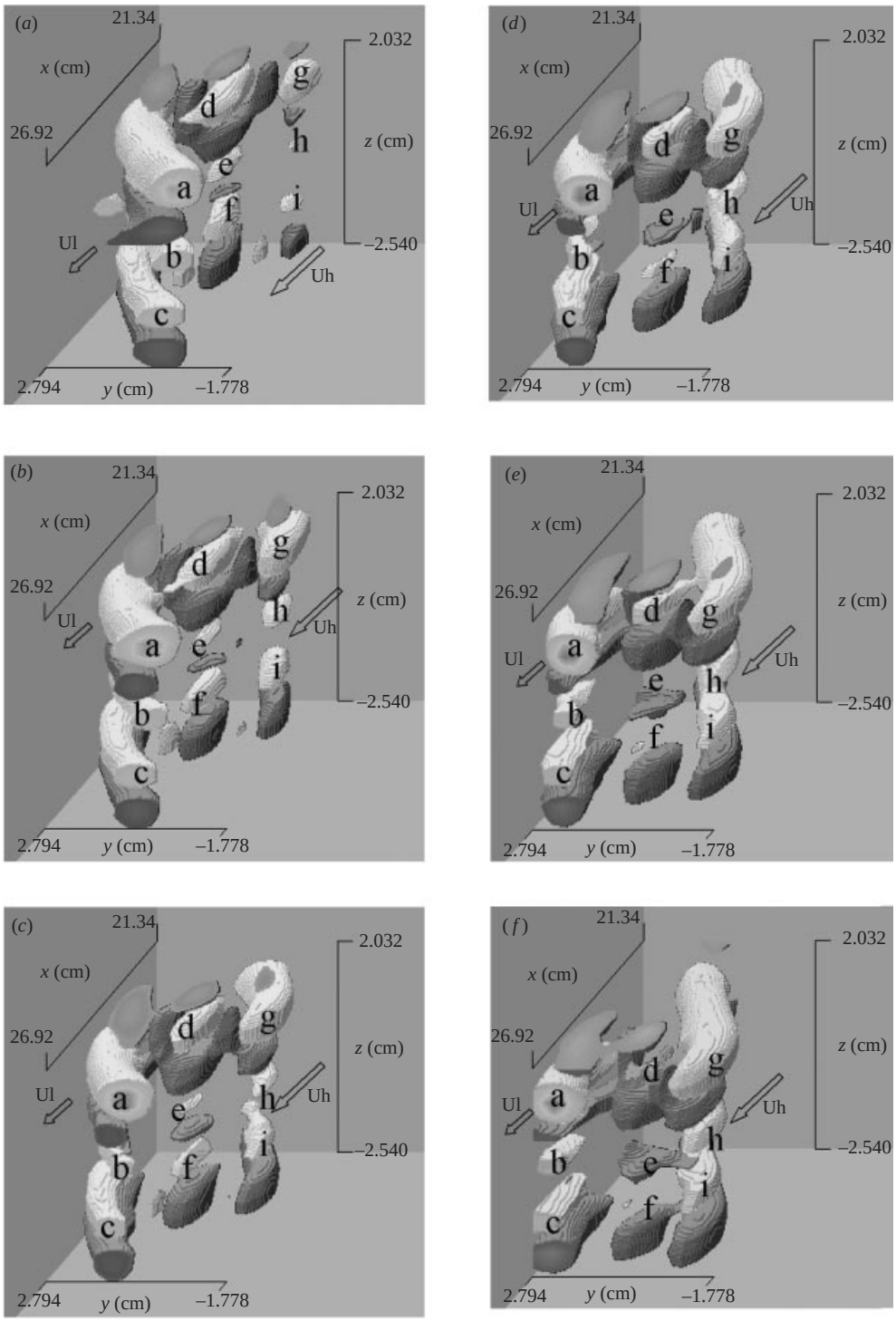

FIGURE 20. Iso-surfaces of phase-averaged streamwise vorticity, $\langle \omega_x \rangle = 50\,\mathrm{s}^{-1}$ (light) and $-50\,\mathrm{s}^{-1}$ (dark), corresponding to frames of figure 11. High-speed (Uh) and low-speed (Ul) sides indicated by arrows. (*a*) Phase 12, (*b*) phase 13, (*c*) phase 14, (*d*) phase 15, (*e*) phase 16, (*f*) phase 17.

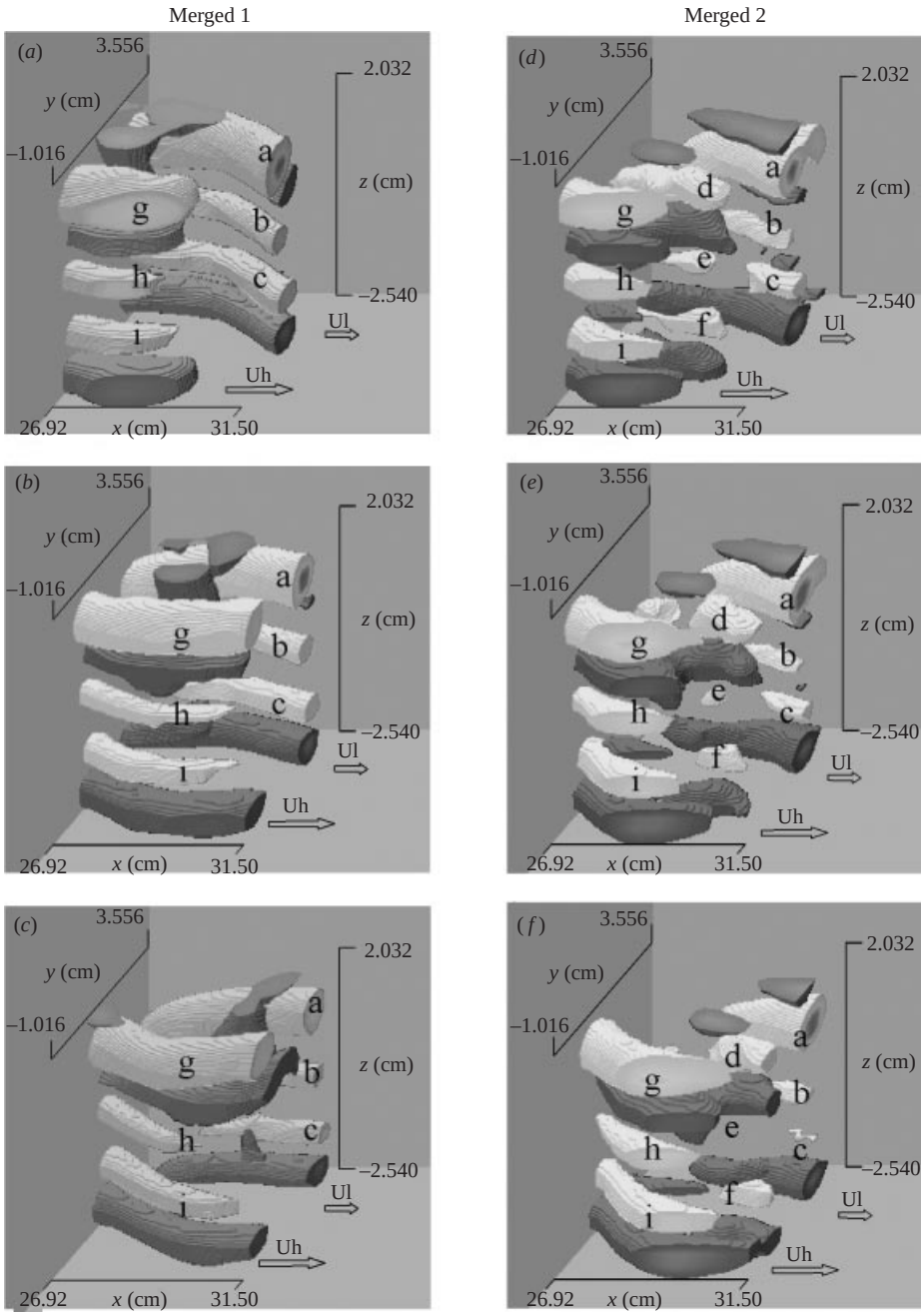

FIGURE 21. Iso-surfaces of phase-averaged streamwise vorticity, $\langle\omega_x\rangle = 50\,\mathrm{s}^{-1}$ (light) and $-50\,\mathrm{s}^{-1}$ (dark), corresponding to merged 1 and 2 of figure 12. High-speed (Uh) and low-speed (Ul) sides indicated by arrows. (*a*) Phase 1, (*b*) phase 3, (*c*) phase 5, (*d*) phase 12, (*e*) phase 13, (*f*) phase 14.

and undergoes amplification as the rollers continue to approach each other. Toward the 90° position, the inner core or centre of the rollers develops bulging-like waves that are out-of-phase with respect to each other. The out-of-phase waves are similar to the helical pairing of two planar vortex waves, as defined by Pierrehumbert &

Widnall (1982). They referred to the pairing as helical because it caused the vortices to twist around each other. In the present study the pairing was not helical in the first grid when the rollers remained planar; rather, the bulging axisymmetric mode was responsible for the out-of-phase roller waves. When the pairing occurred sufficiently downstream, non-axisymmetric waves developed and caused the merging structure to be corrugated.

For a sufficiently upstream pairing location, pairing occurred axisymmetrically. It was found that as the rollers come into contact with each other, their cores exhibit a mildly bulged nature. Amplification of this bulging mode (especially in the weaker low-speed-side roller) causes the spanwise waves to change from in-phase to out-of-phase, and pairing occurs first in the crests of the waves, forming 'bridges' between the rollers. These bridges are three-dimensional, with strong spanwise vorticity. The most noticeable bridge appeared in the area of the strongest roller kink. The resulting merged vortex is quasi-two-dimensional (straight axis). When the pairing occurred sufficiently far downstream, the rollers appeared to be much more corrugated, and non-axisymmetric modes were also amplified.

Local bridging was accompanied by the engulfment of the secondary counter-rotating structures of the shrinking braid. The spanwise rollers were streamwise tilted, with alternating sign of streamwise vorticity along the span. Cross-cuts normal to the streamwise direction through the spanwise rollers revealed quadrupole configurations of the streamwise vorticity at the initiation of pairing. In that formation every vortex is surrounded by vortices of opposite sign, and mini mixing layers are generated in the middle of each. This is consistent with the sign of the streamwise vorticity and the tilting of the rollers. The relative position of the two types of structures was shown by superimposing spanwise and streamwise vorticity fields. The secondary structures appeared to be separated by the peaks and valleys of the peripheral wave of the roller cores. Accordingly, the distance between counter-rotating pairs matched the spanwise wavelength of the rollers. The connection between the secondary and the spanwise structures occurs on their periphery, as the braid wraps around the spanwise rollers. Although the vorticity level is lower in the periphery of these structures, the two types of structures are locked temporally and spatially. Therefore, the phase-averaged measurements educed both types of structures, although only the two-dimensional spanwise structures were artificially stabilized.

The origin of the initial instability of the rollers was related to a kink in the rollers at a specific spanwise location; the kink location was traced back to an upstream localized perturbation (a small imperfection in the splitter plate). Previous studies have shown that kinks from defects in the facility amplify the inherent instabilities of the mixing layer (Jimenez 1983; Bernal & Roshko 1986; Tung & Kleis 1996; Estevadeordal & Kleis 1999*a*, *b*). It is noteworthy that these local perturbations are small and lead to instabilities, with initial growth being consistent with linear-theory predictions (Metcalfe *et al.* 1987; Rogers & Moser 1992). This facilitated phase-averaged experiments where the three-dimensional motions could be set to occur at specific locations periodically.

The connection and interaction between the spanwise and streamwise structures have been investigated and modelled in several studies. Bernal & Roshko (1986) constructed a model based on a continuous vortex line that connects both structures. Hussain (1986) suggested that the interaction of orthogonal spanwise and secondary structures produces three-dimensional turbulence and mixing. Huang & Ho (1990) found that random small-scale eddies were produced by the interactions between the merging spanwise structures and the secondary structures. Tung (1992) observed

turbulent bursting (high-frequency, low-amplitude components) from hot-wire time traces; bursts appeared first within the core of the merged structure. He suggested that the complicated flow pattern established by the counter-rotating secondary structures in the core region was responsible for the bursting. The bursting occurred in a later stage of pairing when the new merged structure was forming. Schoppa *et al.* (1995) suggested that a spanwise core instability corresponding to the bulging mode is one of the main mechanisms responsible for bursting and turbulence transition. The present results show that the three-dimensional activity is highest between the pairing rollers and the more complex shrinking braid; this generates the reported high frequencies and accounts for the observed bursting. The exact mechanism governing the disappearance of the shrinking braid into the merging structure is unknown, but a three-dimensional tearing mechanism is suggested here; this is reinforced by the fact that the bridges of the local pairing have a strong spanwise vorticity component. Viscous vortex reconnection (Moser & Rogers 1993) is another three-dimensional mechanism that may be involved in pairing. Also termed cut-and-connect or cross-linking (Melander & Hussain 1989), this mechanism requires that opposite-sign vorticity regions approach each other and form 'bridges' (Ashurst & Meiron 1987; Kida & Takaoka 1987); in this way the spanwise and secondary structures, being orthogonal to each other, may enhance the chances of reconnection. The present results show that pairing occurs locally and that bridges (indicated by iso-vorticity surfaces) connecting different portions of the rollers are formed. However, the relation of pairing and bridging through reconnection has not been investigated.

The editorial assistance of Ms M. Whitaker of ISSI is greatly appreciated.

REFERENCES

Ashurst, W. T. & Meiron, D. I. 1987 Numerical study of vortex reconnection. *Phys. Rev. Lett.* **58**, 1632–1639.

Bell, J. H. & Mehta, R. D. 1992 Measurements of the streamwise vortical structures in a plane mixing layer. *J. Fluid Mech.* **239**, 213–248.

Bell, J. H. & Mehta, R. D. 1993 Effects of imposed spanwise perturbations on plane mixing-layer structure. *J. Fluid Mech.* **257**, 33–63.

Benney, D. J. & Lin, C. C. 1960 On the secondary motion induced by oscillations in shear flow. *Phys. Fluids* **3**, 656–657.

Bernal, L. P. & Roshko, A. 1986 Streamwise vortex structure in plane mixing layers. *J. Fluid Mech.* **170**, 499–525.

Breidenthal, R. 1980 Response of plane shear layers and wakes to strong three-dimensional disturbances. *Phys. Fluids* **23**, 1929–1934.

Breidenthal, R. 1981 Structure in turbulent mixing layers and wakes using a chemical reaction. *J. Fluid Mech.* **109**, 1–24.

Browand, F. K. 1966 An experimental investigation of the instability of an incompressible separated shear layer. *J. Fluid Mech.* **26**, 281–307.

Browand, F. K. & Troutt, T. R. 1980 A note on spanwise structure in the two-dimensional mixing layer. *J. Fluid Mech.* **117**, 771–781.

Browand, F. K., & Troutt, T. R. 1985 The turbulent mixing layer: geometry of large vortices. *J. Fluid Mech.* **158**, 489–509.

Brown, G. L. & Roshko, A. 1974 On the density effects and large structures in turbulent mixing layers. *J. Fluid Mech.* **64**, 775–816.

Chandrsuda, C. , Mehta, R. D., Weir, A. D. & Bradshaw, P. 1978 Effect of free-stream turbulence on large structure in the turbulent mixing layers. *J. Fluid Mech.* **85**, 693–707.

Collis, S. S., Lele, S. K., Moser, R. D. & Rogers, M. M. 1994 The evolution of a plane mixing layer with spanwise nonuniform forcing. *Phys. Fluids* **6**, 381–396.

Comte, P., Lesieur, M. & Lamballais, E. 1992 Large- and small-scale stirring of vorticity and a passive scalar in a three-dimensional temporal mixing layer. *Phys. Fluids* A **4**, 2761–2778.

Estevadeordal, J. & Kleis, S. J. 1999*a* Core instabilities and 'bridging' in the first pairing of plane mixing layers. *Phys. Fluids* **11**, 1688–1690.

Estevadeordal, J. & Kleis, S. J. 1999*b* Double-helical pairing in plane mixing layers. *Phys. Fluids* **11**, 1691–1693.

Estevadeordal, J. & Kleis, S. J. 1999*c* High-resolution measurements of two-dimensional instabilities and turbulence transition in plane mixing layers. *Exps. Fluids* **27**, 378–390.

Ho, C. M. & Huang, L.-S. 1982 Subharmonic and vortex merging in mixing layers. *J. Fluid Mech.* **119**, 443–473.

Huang, L. S. & Ho, C.-M. H. 1990 Small-scale transition in a plane mixing layer. *J. Fluid Mech.* **210**, 475–500.

Hussain, A. K. M. F. 1986 Coherent structures and turbulence. *J. Fluid Mech.* **173**, 303–356.

Jeong, J. & Hussain, F. 1995 On the identification of a vortex. *J. Fluid Mech.* **285**, 69–94.

Jimenez, J. 1983 A spanwise structure in the plane shear layer. *J. Fluid Mech.* **132**, 319–336.

Kida, S. & Takaoka, M. 1987 Bridging in vortex reconnection. *Phys. Fluids* **30**, 2911–2914.

Lasheras, J. C., Cho, J. S. & Maxworthy, T. 1986 On the origin and evolution of streamwise vortical structures in a plane, free shear layer. *J. Fluid Mech.* **172**, 231–258.

Lasheras, J. C. & Choi, H. 1988 Three-dimensional instability of a plane free shear layer: an experimental study of the formation and evolution of streamwise vortices. *J. Fluid Mech.* **189**, 53–86.

Leboeuf, R. L. & Mehta, R. D. 1993 Streamwise vortex meander in a plane mixing layer. *Phys. Fluids* A **5**, 1983–1991.

Leboeuf, R. L. & Mehta, R. D. 1995 Measurements of spanwise scale change in a forced mixing layer. *J. Fluid Mech.* **293**, 305–319.

Leboeuf, R. L. & Mehta, R. D. 1996 Vortical structure morphology in the initial region of a forced mixing layer: roll-up and pairing. *J. Fluid Mech.* **315**, 175–221.

Lin, S. J. & Corcos, G. M. 1984 The mixing layer: deterministic models of a turbulent flow. Part 3. The effect of plane strain on the dynamics of streamwise vortices. *J. Fluid Mech.* **141**, 139–178.

Melander, M. V. & Hussain, F. 1989 Cross-linking of two antiparallel vortex tubes. *Phys. Fluids* A **1**, 633–636.

Metcalfe, R. W., Orszag, S. A., Brachet, M. E., Menon, S. & Riley, J. J. 1987 Secondary instability of a temporally growing mixing layer. *J. Fluid Mech.* **184**, 207–247.

Miksad, R. W. 1972 Experiments in the non-linear stages of free-shear-layer transition. *J. Fluid Mech.* **56**, 695–719.

Moser, R. D. & Rogers, M. M. 1991 Mixing transition and the cascade to small scales in a plane mixing layer. *Phys. Fluids* A **3**, 1128–1134.

Moser, R. D. & Rogers, M. M. 1993 The three-dimensional evolution of a plane mixing layer: pairing and transition to turbulence. *J. Fluid Mech.* **247**, 275–320.

Nygaard, K. J. & Glezer, A. 1991 Evolution of streamwise vortices and generation of small-scale motion in a plane mixing layer. *J. Fluid Mech.* **231**, 257–301.

Nygaard, K. J. & Glezer, A. 1994 The effect of phase variations and cross-shear on vortical structures in a plane mixing layer. *J. Fluid Mech.* **276**, 21–59.

Pierrehumbert, R. T. & Widnall, S. E. 1982 The two- and three-dimensional instabilities of a spatially periodic shear layer. *J. Fluid Mech.* **114**, 59–82.

Rogers, M. M. & Moser, R. D. 1992 The three-dimensional evolution of a plane mixing layer: the Kelvin–Helmholtz rollup. *J. Fluid Mech.* **243**, 183–226.

Rogers, M. M. & Moser, R. D. 1993 Spanwise scale selection in plane mixing layers. *J. Fluid Mech.* **247**, 321-337.

Schoppa, W., Hussain, F. & Metcalfe, R. W. 1995 A new mechanism of small-scale transition in a plane mixing layer: core dynamics of spanwise vortices. *J. Fluid Mech.* **298**, 23–80.

Tung, C. H. 1992 Initial streamwise formation in a plane mixing layer. PhD thesis, University of Houston, Houston, TX.

Tung, S. & Kleis, S. J. 1996 Initial streamwise vorticity formation in a two-stream mixing layer. *J. Fluid Mech.* **319**, 251–279.

WINANT, C. D. & BROWAND, F. K. 1974 Vortex pairing: the mechanism of turbulent mixing-layer growth at moderate Reynolds number. *J. Fluid Mech.* **63**, 237–255.

WYGNANSKI, I., OSTER, D., FIEDLER, H. & DZIOMBA, B. 1979 On the perseverance of a quasi-two-dimensional eddy-structure in a turbulent mixing layer. *J. Fluid Mech.* **93**, 325–335.

ZAMAN, K. B. M. Q. & HUSSAIN, A. K. M. F. 1981 Taylor hypothesis and large-scale coherent structures. *J. Fluid Mech.* **112**, 379–396.